Posted on 31 Jan 2024 — The copyright holder is the author/funder. All rights reserved. No reuse without permission. — https://doi.org/10.22541/au.170669107.72727336/v1 — This is a preprint and has not been peer-reviewed. Data may be preliminary.

Fabrication of hierarchical CoP/ZnCdS/Co3O4 quantum dots bi-heterostructure cages foreefficient hydrogen evolution

Yanbing Li[1], PENGFEI ZHU[2], Zhiliang Jin[3], and Noritatsu Tsubaki[1]

[1]University of Toyama
[2]Shaanxi University of Science and Technology
[3]Affiliation not available

April 16, 2024

Abstract

The design and construction of hierarchical CoP/ZnCdS/Co3O4 quantum dots (QDs) (800>40>4.5 nm) bi-heterostructure cages as an ultrahigh-performance photocatalyst for hydrogen evolution with visible light is investigated. Three excellent photoactive materials that ZnCdS solid solution, high-conductivity CoP and high-efficiency Co3O4 QDs were integrated into a all-in-one bi-heterostructure cage architecture. Presence of the two high-efficiency electron-transfer pathways in CoP/ZnCdS/Co3O4 QDs can seriously facilitate the separation and migration of light-induced electrons while the unique structure also can offer large reaction surface and expose abundant active sites for photocatalytic hydrogen evolution reaction. Because of the distinctively compositional and structural merits, the hierarchical CoP/ZnCdS/Co3O4 QDs bi-heterostructure cages without introducing any cocatalysts exhibit ultrahigh activity and favorable stability for generation of high-purity hydrogen under visible light irradiation.

Fabrication ofhierarchicalCoP/ZnCdS/Co_3O_4quantum dots (800>40>4.5 nm) bi-heterostructure cages for efficient photocatalytic hydrogen evolution

Yanbing Li [a], Pengfei Zhu [c], Zhiliang Jin [b]*, Noritatsu Tsubaki [a]*

a. Department of Applied Chemistry, School of Engineering, University of Toyama, Gofuku 3190, Toyama 930-8555, Japan

b. School of Chemistry and Chemical Engineering,North Minzu University, Yinchuan 750021, PR China

c. School of Environmental Science and Engineering, Shaanxi University of Science and Technology, Xi'an, 710021, Shanxi, China.

Corresponding author:*zl-jin@nun.edu.cn* (Z.L. Jin);*tsubaki@eng.u-toyama.ac.jp*(N. Tsubaki)

Abstract: The design and construction of hierarchical CoP/ZnCdS/Co_3O_4quantum dots (QDs) (800>40>4.5 nm) bi-heterostructure cages as an ultrahigh-performance photocatalyst for hydrogen evolution with visible light is investigated. Three excellent photoactive materials that ZnCdS solid solution, high-conductivity CoP and high-efficiency Co_3O_4 QDs were integrated into a all-in-one bi-heterostructure cage architecture. Presence of the two high-efficiency electron-transfer pathways in CoP/ZnCdS/Co_3O_4 QDs can seriously facilitate the separation and migration of light-induced electrons while the unique structure also can offer large reaction surface and expose abundant active sites for photocatalytic hydrogen evolution reaction. Because of the distinctively compositional and structural merits, the hierarchical CoP/ZnCdS/Co_3O_4 QDs bi-heterostructure cages without introducing any cocatalysts exhibit ultrahigh activity and favorable stability for generation of high-purity hydrogen under visible light irradiation.

Posted on 31 Jan 2024 — The copyright holder is the author/funder. All rights reserved. No reuse without permission. — https://doi.org/10.22541/au.170669107.72727336/v1 — This is a preprint and has not been peer-reviewed. Data may be preliminary.

Key words: CoP/ZnCdS/Co_3O_4; quantum dots; bi-heterostructure; hydrogen generation.

Introduction

Overexploitation and hence the ever growing depletion of fossil fuels, in addition to the anthropogenic climate change caused by the release of greenhouse gases by combustion of these nature resources is a matter of profound concern because more than 80% of the world energy requirement still is derived from fossil fuels at present [1-3]. Thus, it is urgent to develop renewable energy resources. Of the green alternative energy resources available, hydrogen energy from solar energy and water is arguably the most promising one because of its merits of green, high energy density, renewable [4-7]. However, the low separation and migration efficiency of charge carriers greatly restrict the water-splitting properties of semiconductor photocatalysts. Therefore, in order to meet the dawn of the practical application of hydrogen energy from solar energy and water earlier, improving seriously hydrogen generation rate via designing and constructing more efficient functional semiconductor materials still is a key subject up to now.

Metal chalcogenide semiconductor photocatalysts, such as CdS, $ZnIn_2S_4$, $Mn_{1-x}Cd_xS$, $Zn_{1-x}Cd_xS$, have attracted considerable attention due to the favorable visible-light response ability [8-12]. Of all sulfide semiconductors, CdS is a well-established photocatalyst for hydrogen evolution due to its appropriate band gap (2.4 eV) and good visible light response performance. However, rapid electron recombination and serious photocorrosion hinder the photocatalytic efficiency and stability of CdS [13]. In order to overcome these shortcomings, CdS-based solid solution semiconductor photocatalysts were constructed, such as $Mn_{1-x}Cd_xS$, and $Zn_{1-x}Cd_xS$, and they have been widely investigated in photocatalytic hydrogen production because of them merits in tunable band gap (2.28˜3.94 eV) for light absorption and optimizeable band edge positions for photo redox reactions [14,15]. But, while the Cd/Zn molar ratio is 1, that is, where x is 0.5, the prepared $Zn_{0.5}Cd_{0.5}S$ nanoparticles possess the best photocatalytic performance among $Zn_{1-x}Cd_xS$ solid solution semiconductors and far exceed alone CdS and ZnS catalysts as well [16]. Nevertheless, the fact that fast electron-hole recombination still exists in the $Zn_{0.5}Cd_{0.5}S$ semiconductor, which would impede the further enhancement of photocatalytic properties of $Zn_{1-x}Cd_xS$ solid solution materials. Consequently, it is to absolutely accelerate the separation and migration of charge carriers that is the vital factor to be overcome for extremely high-efficiency photocatlytic hydrogen evolution.

Transition metal phosphides (TMPs) have arisen as a high-performance class of candidates in photocatalytic water splitting, supercapacitors, and electrochemical energy storage owing to their inherent semi-metallic nature and high electrical conductivity [17-19]. And metal phosphides not only are good conductors of electricity and heat, but also have high chemical stability, so they are kinetically favorable for the rapid charge transfer required for high power density [20,21]. Not only that, they possess these advantages of environmentally benign nature, and high abundance [22]. The negatively charged P on the surface of a metal phosphide could not only trap protons as the base, but also provide high activity for the dissociation of H_2, thus preventing the system from deactivation caused by high coverage of strongly bonding hydrogen atoms [23,24]. Cobalt phosphide (CoP) as one of TMPs has been proven to be high-performance photocatalyst and cocatalyst owing to the coexistence synergism conductive to fast charge transport [25,26].

Three-dimensionally confined quantum dots (QDs) have emerged as new-generation semiconducting materials owing to tunable bandgaps, narrow emission bandwidth, and high efficiency [27]. And their typical dimensions range from nanometres to a few microns, and their size can be precisely controlled. And QDs have these advantages of higher specific surface areas and shorter paths for charge transport [28]. QDs are more widely used in the fields of display, photovoltaic, transistor [29]. Co_3O_4QDs with a size of about 4.5 nm was synthesized by Shi et al. for the first time and applied in efficient oxygen evolution [30]. However, it has few reports in the field of solar-driven water splitting, It was prepared for improved hydrogen evolution that a series of novel quasi 0D/2D CoP/g-C_3N_4 derived from 4.5 nm Co_3O_4 QDs with g-C_3N_4 nanosheets [31]. The construction of Co_3O_4QDs (4.5 nm)/3D hexagonal CdS single crystals p-n heterojunction enhanced photocatalytic hydrogen production [32].

In view of these merits and the application blank in field of photocatalytic hydrogen evolution, 4.5 nm

Posted on 31 Jan 2024 — The copyright holder is the author/funder. All rights reserved. No reuse without permission. — https://doi.org/10.22541/au.170669107.72727336/v1 — This is a preprint and has not been peer-reviewed. Data may be preliminary.

Co_3O_4 QDs involved hierarchical CoP/ZnCdS/Co_3O_4QDs (800>40>4.5 nm) bi-heterostructure cages was reasonably designed and successfully constructed via taking their large differences in size. The architecture aims to build bi-heterojunction structure to greatly accelerate the separation and migration of electron-hole pairs from visible-light-induced ZnCdS solid solution for more high-activity hydrogen evolution reaction, that is, to rapidly migrate charges on the conduction band of ZnCdS from two paths make more excited electrons put into photocatalytic hydrogen reaction.

Experimental section

2.1 Catalyst preparation

2.1.1 Preparation of ZIF-67: ZIF-67 was prepared according to the reference with some modifications [33]. In a typical preparation, two solutions were prepared by dissolving $Co(NO_3)_2{\cdot}6H_2O$ (0.873 g) in 30 mL of methanol and 2-methylimidazole (0.984 mg) in 10 mL of methanol, respectively. And they were completely dissolved with stirring. Subsequently, the two solutions were mixed rapidly and aged for 24 h at room temperature. The synthesized blue precipitate was washed with ethanol 3 times and then dried at 60 °C.

2.2 Preparation of ZIF-67 derived CoP polyhedron: CoP polyhedrons were prepared by annealing the ZIF-67 (0.05 g) with $NaPO_2H_2{*}H_2O$ (0.5 g) in a N_2 flow at 300°C for 2 h with a heating rate of 5 °C min^{-1}. $NaPO_2H_2{*}H_2O$ was placed upstream of N_2, and ZIF-67 was placed downstream.

2.1.2 Preparation of Co_3O_4Quantum Dots: Co_3O_4 quantum dots were prepared by reference to published literature [30,31]. Typically, 0.249 g (1 mmol) of cobalt (II) acetate tetrahydrate [$Co(Ac)_2{*}4H_2O$] was put into round bottom flask containing 7 mL benzyl alcohol. And then the mixture was kept stirring at ambient temperature till $Co(Ac)_2{*}4H_2O$ was completely dissolved. Afterward, 7 mL ammonium hydroxide (25%) solution was dropwise added into the above open reactor under vigorous stirring. The vessel with reddish-brown solution was kept heating in an oil bath set at 165 °C. Then, the solution was getting immediately boiling with a large number of bubbles, and it was kept at 165 °C for 2 h under continuous stirring. Later, a black suspension was formed. Finally, 7 mL diethyl ether was put into the finished reaction suspension under continuous stirring. Subsequently, the black precipitate was washed with ethanol several times via centrifugation until the washing solution becomes clear, and then it was dried at 60 °C.

2.1.3 Preparation of ZnCdS: According to the references [34,35], $Cd_{0.5}Zn_{0.5}S$ solid solution was prepared by a precipitation-hydrothermal means. Typically, both 1.0975 g (5 mmol) zinc acetate dihydrate and 1.3326 g (5 mmol) cadmium acetate dihydrate were dissolved into 40 mL of distilled water in a PTFE vessel (100 mL), and 0.9391 g (12.5 mmol) thioacetamide (TAA) also was added into the vessel under vigorous stirring. After they were completely dissolved, 10 mL NaOH aqueous solution (4 M) was put into the above container and then stirred for 1 h. Subsequently, the sealed autoclave was heated and kept at 180 °C for 24 h. After that, the resulting yellow samples was washed with distilled water and ethanol three times, and then dried at 60 °C.

2.1.4 Fabrication ofCoP/ZnCdS/Co_3O_4Quantum Dots: First, two solutions were prepared by dispersing Co_3O_4 quantum dots (0.01 g) and CoP polyhedrons (0.01 g) in 100 mL ethanol, respectively. And the two solutions were dispersed thoroughly and evenly through ultrasonic and then stirring treatments. Later, 0.1 g ZnCdS was dispersed completely in 60 mL ethanol via ultrasonic treatment, then 15x1000 μL of CoP suspension (1.5 wt.% CoP) was continuously added into the above ZnCdS suspension under vigorous stirring. After it was stirred for half an hour, 15×1000 μL of Co_3O_4quantum dots suspension (1.5 wt.% Co_3O_4quantum dots) also was continuously put into the vessel, and then it was placed in water bath set as 80 °C with vigorous stirring until precipitate was completely separate out. This assembled Co_3O_4 quantum dots (1.5 wt.%) /ZnCdS/CoP (1.5 wt.%) was labeled O/ZCS/P-3. And according to the added content of Co_3O_4 quantum dots, the named O/ZCS/P-1, O/ZCS/P-2, and O/ZCS/P-4 correspond to 5×1000 μL (0.5 wt.%), 10×1000 μL (1.0 wt.%), and 20×1000 μL (2.0 wt.%) of Co_3O_4quantum dots suspension, respectively. And the content of CoP in O/ZCS/P samples were arranged as 1.5 wt.% (15×1000 μL of CoP suspension).

Posted on 31 Jan 2024 — The copyright holder is the author/funder. All rights reserved. No reuse without permission. — https://doi.org/10.22541/au.170669107.72727336/v1 — This is a preprint and has not been peer-reviewed. Data may be preliminary.

2.1.5 Fabrication of ZnCdS/CoP: The synthesis of ZnCdS/CoP was same as those of O/ZCS/P in the absence of Co_3O_4 quantum dots. 5×1000 μL (0.5 wt.%), 10×1000 μL (1.0 wt.%), 15×1000 μL (1.5 wt.%) and 20×1000 μL (2.0 wt.%) of CoP suspension was added into 60 mL ZnCdS (0.1 g) suspension, respectively. After the same experiment as above, the obtained ZnCdS/CoP samples were named ZnCdS/CoP-1, ZnCdS/CoP-2, ZnCdS/CoP-3, and ZnCdS/CoP-4 in turn.

2.2 Characterization of catalysts: The crystalline and phase information were obtained by taking a Rigaku RINT-2000 diffractometer. The geometric features of the obtained catalysts were investigated by JSM-6701F JEOL FESEM (Field-Emission Scanning Electron Microscope) and JEM1200EX JEOL TEM (Transmission Electron Microscopy). The Brunauer-Emmett-Teller (BET) specific surface area (S_{BET}) of powers were analyzed on an ASAP 2460 analyzer equipped with Vac Prep 061 sample degas system. X-ray photoelectron spectroscopy (XPS) of elements were performed on an ESCALAB 250Xi. Uv-visible diffuse reflectance spectra (UV-vis DRS) were studied on UV-2550 spectrophotometer. The fluorescence curves for the resulting photocatalysts were tested on FLUOROMAX-4 fuorescence spectrometer. The photoelectrochemical tests (I-T, EIS, LSV) for were measured on VersaStat4-400 electrochemical workstation equipped with a standard three electrode cell, and Pt sheet with 2*2 cm^2 is for counter electrode, saturated calomel electrode (SCE) is for reference electrode, 0.2 mol/L Na_2SO_4 aqueous solution is to be electrolyte, ITO (1*2 cm^2) drop-coating photocatalyst (1*1 cm^2) was acted as working electrode, respectively. A light source for I-T measures is to be 300W xenon lamp.

2.3 Photocatalytic hydrogen evolution experiments: The assessment of photocatalytic hydrogen evolution performance of the obtained catalysts were proceeded in anaerobic system. Typically, 10 mg of sample was ultrasonically suspended into 30 mL of aqueous solution containing lactic acid solution (10 vol.%) as the sacrificial reagent. Prior to exerting light, the reactor was degassed with ready $N_2$to thoroughly exclude the air and the dissolved oxygen in reaction system. Then, the enclosed reactor was paced in a nine-channel photocatalytic reaction system equipped with 5 W LED as a light to generate H_2, and the produced H_2 was detected on a Tianmei GC7900 gas chromatograph (TCD, 13Xcolumn).

3. Results and Discussion

3.1 Synthesis of CoP/ZnCdS/Co_3O_4QDs

Herein, we demonstrate the rational design and construction of hierarchical CoP/ZnCdS/Co_3O_4QDs bi-heterostructure cages by assembling about 800 nm CoP polyhedrons, 40 nm ZnCdS, and 4.5 nm Co_3O_4 QDs as a prominent photocatalyst for H_2 evolution. The overall synthetic route for constructing the delicate architectures is schematically illustrated in Fig. 1. Starting with ZIF-67 dodecahedrons as the precursor, CoP polyhedrons with large surface was gained via phosphatizing reaction. In addition, ZnCdS nanoparticles and Co_3O_4 QDs are synthesized via solvothermal methods. Finally, the two cages, CoP/ZnCdS heterostructure cage with 40 nm ZnCdS nanoparticles coated on the surface of about 800 nm CoP polyhedron and ZnCdS/Co_3O_4 QDs cages with 4.5 nm Co_3O_4 QDs decorated on the surface of 40 nm ZnCdS nanoparticle, are integrated into all-in-one hierarchical CoP/ZnCdS/Co_3O_4QDs bi-heterostructure cages via utilizing their pyramid-shaped size distribution. The complex CoP/ZnCdS/Co_3O_4 QDs bi-heterostructure cage architectures with excellent metal phosphide, solid solution, and quantum dot subunits can seriously accelerate the separation and transfer of electron-hole pairs, offer large surface area, and expose a lot of active sites for photocatalytic H_2 production. Accordingly, the optimum CoP/ZnCdS/Co_3O_4QDs bi-heterostructure cages reveal ultrahigh activity and high stability for visible light driven water splitting.

Posted on 31 Jan 2024 — The copyright holder is the author/funder. All rights reserved. No reuse without permission. — https://doi.org/10.22541/au.170669107.72727336/v1 — This is a preprint and has not been peer-reviewed. Data may be preliminary.

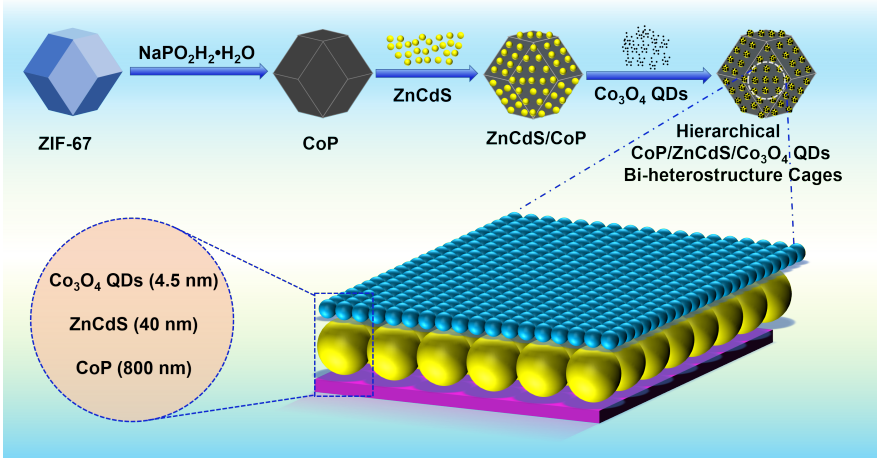

Fig. 1 Schematic presentation of the synthetic route of hierarchical CoP/ZCS/Co_3O_4 QDs bi-heterostructure cages.

3.2 Morphology and structure of as-prepared photocatalysts

FESEM image in Fig. 2a shows the delicate ZIF-67 dodecahedron particles. And Fig. 2b manifests that CoP particles with the size of about 800 nm well inherit the polyhedral morphology of their ZIF-67 precursors, but its surface is concave inward and many cracks are formed on the surface of CoP polyhedron due to the porous characteristics of metal organic frameworks (MOFs). ZnCdS nanaoparticles exhibit an average size of approximately 40 nm (Fig. 2c). The FESEM image of ZnCdS/Co_3O_4QDs heterostructure cages also was investigated as shown in Fig. 2d. However, Co_3O_4QDs can't be observed in the FESEM image (Fig. 2e) because its size is only about 4.5 nm as shown in the TEM image (Fig. 2f), but the existence of Co_3O_4 QDs is proved via EDS and element mapping tests. In Fig. 2g, in addition to Zn (23.52 wt.%), Cd (39.24 wt.%) and S (26.03 wt.%) elements were detected in the micro-scale testing area, Co species (0.94 wt.%) also were identified, which is consistent with the performed results of element mapping as displayed Fig. 2h. And the density of Co element obviously is lower in comparison with that of Zn, Cd, and S elements. These results signify the ZnCdS/Co_3O_4QDs heterostructure cages can be rationally designed and successfully constructed via fabricating Co_3O_4 QDs having only the average size of 4.5 nm on the surface of ZnCdS nanoparticles with the average size of 40 nm. Furthermore, it can be seen from Fig. 2i that the architecture of hierarchical CoP/ZnCdS/Co_3O_4 QDs bi-heterostructure cages was successfully constructed, just as we have wanted. Namely, ZnCdS nanoparticles were decorated on the surface of CoP polyhedron while Co_3O_4 QDs were integrated into the surface of ZnCdS nanoparticles to form hierarchical CoP/ZnCdS/Co_3O_4 QDs double cage heterostructures. In Fig. 2l, a set of distinct lattice fringes with spacing of 0.32 nm can be identified as the (002) planes of ZnCdS solid solution, and the lattice fringes of CoP and Co_3O_4 QDs are not observed because of their low crystallinity and content, consistent with the XRD analysis (Fig. 3a,b). And these elements of Zn, Cd, S, Co and P can be clearly observed in EDS (Fig. 2j) and element mapping images (Fig. 2m), and they are distributed uniformly.

Posted on 31 Jan 2024 — The copyright holder is the author/funder. All rights reserved. No reuse without permission. — https://doi.org/10.22541/au.170669107.72727336/v1 — This is a preprint and has not been peer-reviewed. Data may be preliminary.

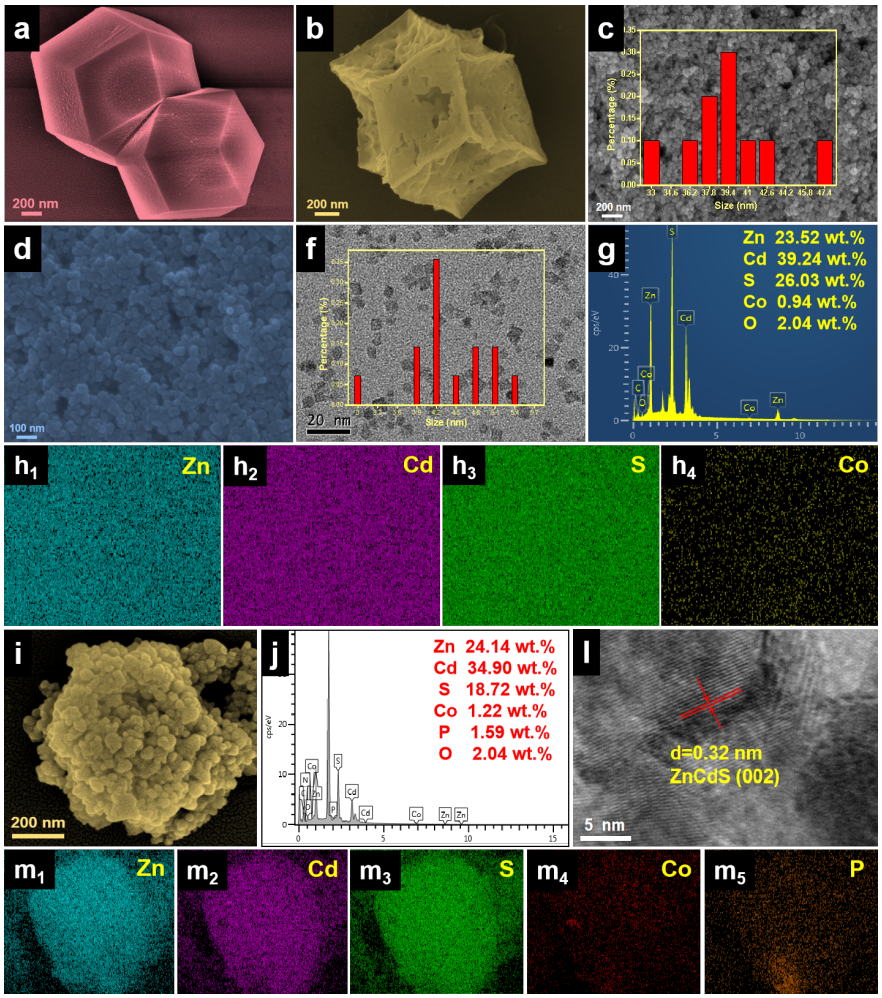

Fig. 2 FESEM images of (a) ZIF-67, (b) CoP polyhedron, (c) ZnCdS, and (d) ZnCdS/Co_3O_4 QDs; (f) TEM image of Co_3O_4 QDs; (g, h) EDS and element mapping images of ZnCdS/Co_3O_4QDs; (i) FESEM images of CoP/ZnCdS/Co_3O_4QDs; (j-m) EDS, HRTEM, and element mapping images of CoP/ZnCdS/Co_3O_4 QDs.

3.3 Phase structure and surface chemical state

The Co_3O_4 QDs, CoP, ZCS and O/ZCS/P-x samples were further performed by X-ray diffraction (XRD) to determine the phase composition. As displayed in Fig. 3a, the XRD pattern of Co_3O_4 QDs matches well with cubic phase Co_3O_4 (PDF#42-1467) [30], and the characteristic peaks at 36.6°, 44.8°, 59.4° and 65.1° can be severally indexed to the (311), (400), (511) and (440) crystal planes of cubic phase Co_3O_4. Meanwhile, the diffraction peaks at 31.6°, 36.2°, 48.1° and 56.7° in the XRD pattern of the bare CoP were in accordance with the (011), (111), (211) and (212) crystal planes of orthorhombic CoP (PDF#29-497) [36,37]. Fig. 3b displays the XRD patterns of ZCS and ZCS-based hybrids. The representative diffraction peaks of at 26.1°, 27.8°, 29.5°, 38.4°, 45.9°, 50.2° and 54.5° can be severally indexed to the (100), (002), (101), (102), (110), (103) and (112) crystal planes of hexagonal $Zn_{0.5}Cd_{0.5}S$ (PDF #89-2943) [38]. However, no visible diffraction peaks of $Co_3O_4$and CoP were presented in all ZCS-based samples, which is because of the extremely low content and crystallinity of Co_3O_4 and CoP. Nevertheless, the presence of Co_3O_4 and CoP in the O/ZCS/P-x composites has been proved by EDS and element mapping techniques as displayed in Fig. 2.

The X-ray photoelectron spectroscopy (XPS) was applied to investigate the surface composition and chemical

states of the as-obtained samples. The Co 2p and O 1s high-resolution XPS profiles of original Co_3O_4 QDs are illustrated in Fig. 3c and d, respectively. The two peaks at 780.2 and 795.5 eV are attributed to Co $2p_{3/2}$ and Co $2p_{1/2}$ of Co^{2+}, and other two peaks at 782.1 and 797.9 eV are assigned to Co $2p_{3/2}$ and Co $2p_{1/2}$ of Co^{3+} [39], respectively. The peaks centered at 530.0 and 531.6 eV in the O 1 s XPS profiles of Co_3O_4 QDs belong to Co-OH and Co-O groups, respectively. And the signals at 787.8 and 804.1 eV correspond to the satellite peaks of Co $2p_{3/2}$ and Co $2p_{1/2}$, respectively. The Co 2p and P 2p high-resolution spectrum of pristine CoP are displayed in Fig. 3e. The XPS spectrum of Co 2p in CoP is similar to that in Co_3O_4 QDs, but it is very clearly that the binding energies of both Co^{2+} and Co^{3+} in Co 2p are bigger than those in Co_3O_4 QDs, which is due to the stronger electronegativity P elements in CoP. The weak signals at 129.5 and 130.3 eV in the high-resolution spectrum of P 2p (Fig. 3f) belong to the index of Co-P bonds in CoP [40]. While the peak at 134.1 eV is attributed to the oxidized P owing to the inevitable surface oxidation.

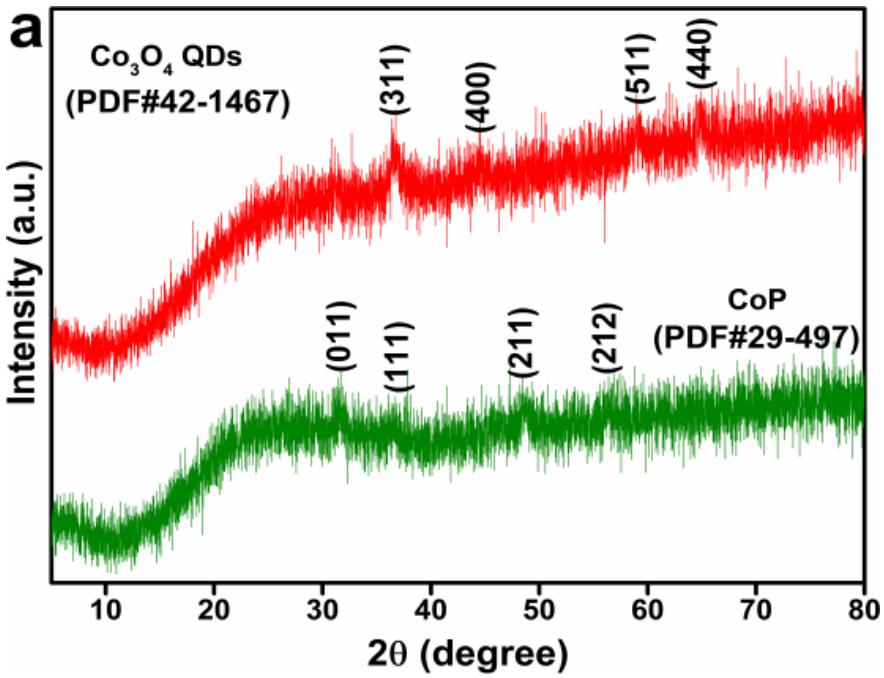

Posted on 31 Jan 2024 — The copyright holder is the author/funder. All rights reserved. No reuse without permission. — https://doi.org/10.22541/au.170669107.72727336/v1 — This is a preprint and has not been peer-reviewed. Data may be preliminary.

Posted on 31 Jan 2024 — The copyright holder is the author/funder. All rights reserved. No reuse without permission. — https://doi.org/10.22541/au.170669107.72727336/v1 — This is a preprint and has not been peer-reviewed. Data may be preliminary.

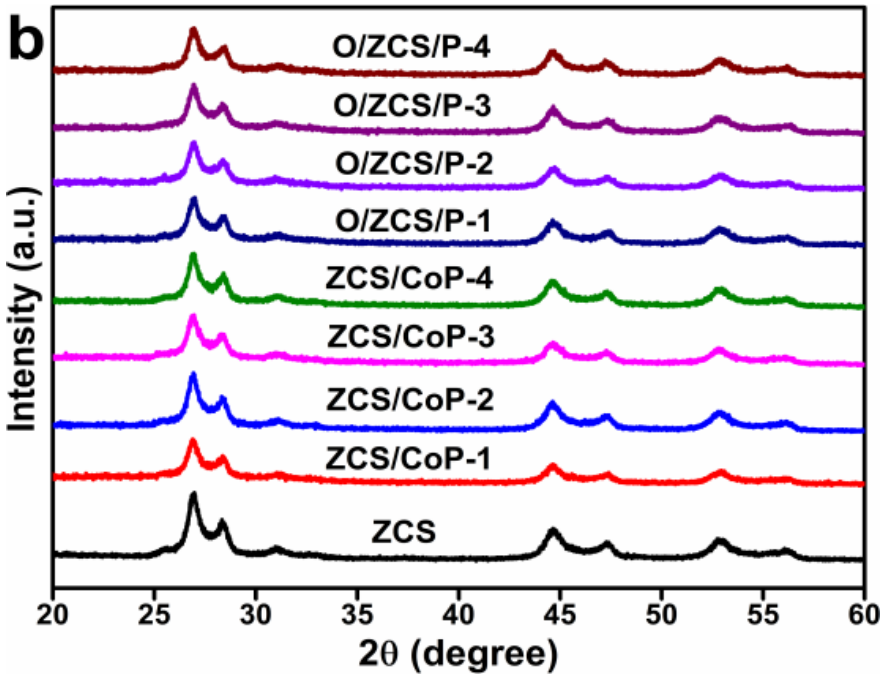

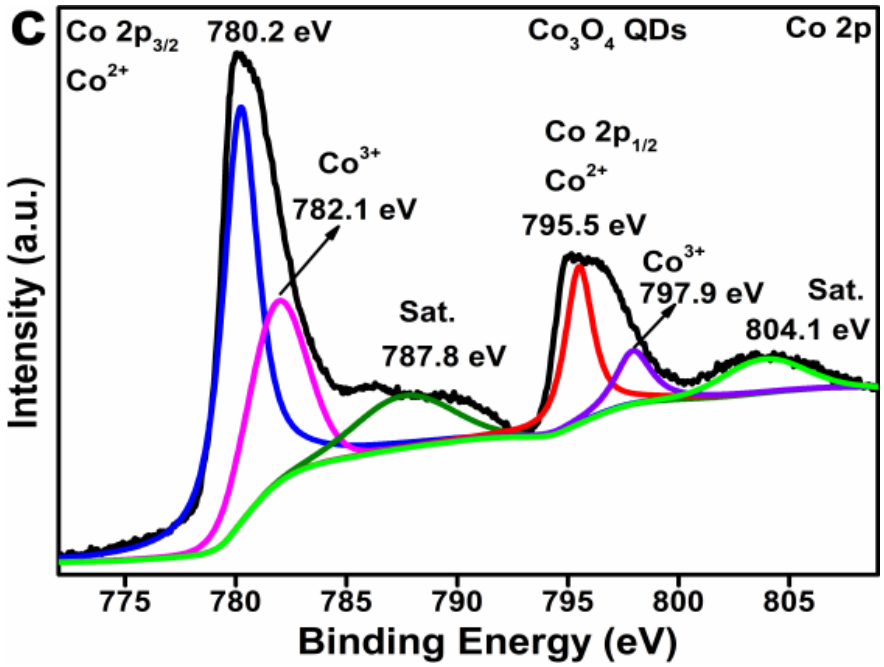

Posted on 31 Jan 2024 — The copyright holder is the author/funder. All rights reserved. No reuse without permission. — https://doi.org/10.22541/au.170669107.72727336/v1 — This is a preprint and has not been peer-reviewed. Data may be preliminary.

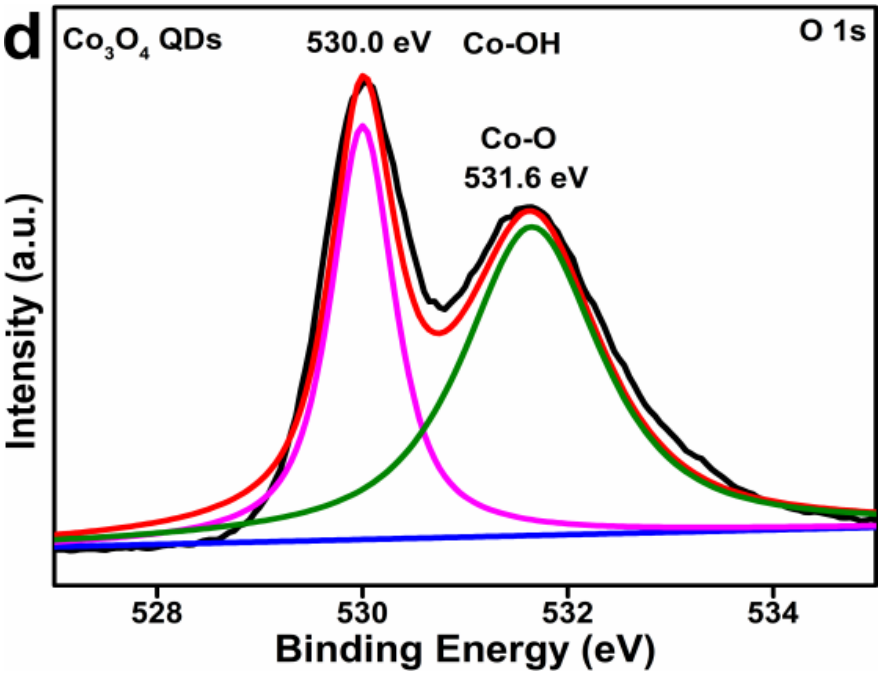

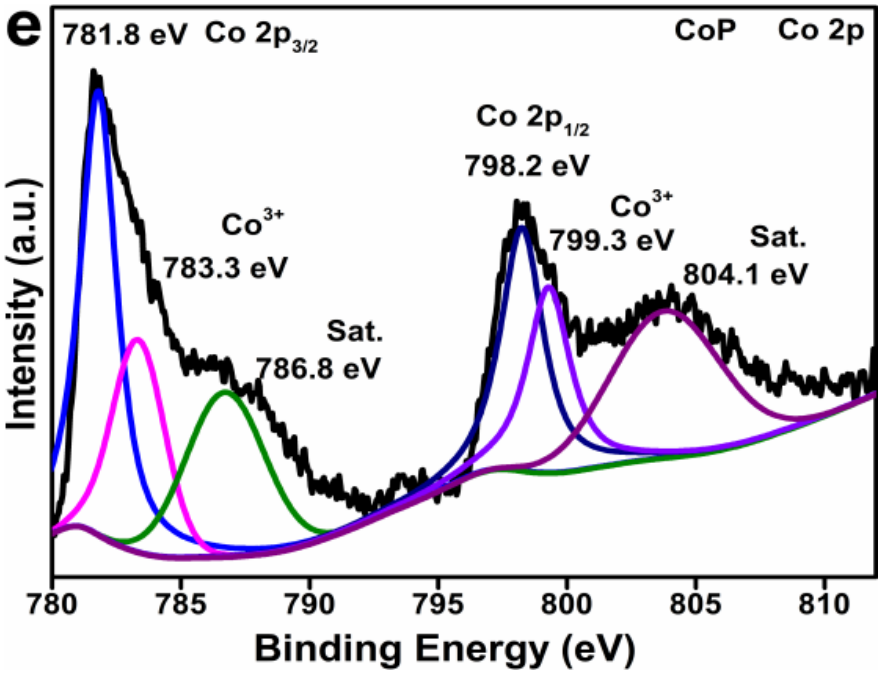

Posted on 31 Jan 2024 — The copyright holder is the author/funder. All rights reserved. No reuse without permission. — https://doi.org/10.22541/au.170669107.72727336/v1 — This is a preprint and has not been peer-reviewed. Data may be preliminary.

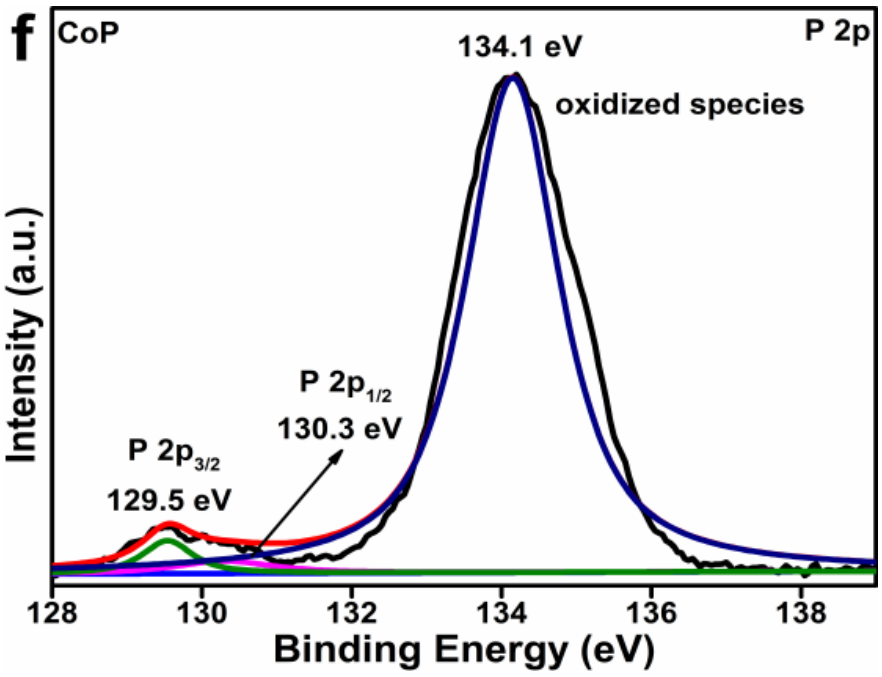

Fig. 3 XRD patterns of (a) CoP, Co_3O_4 QDs, and (b) ZCS, ZCS/CoP-x and O/ZCS/P-x samples; XPS spectra of (c) Co 2p and O 1s for Co_3O_4 QDs, and (d) Co 2p and P 2p for CoP.

In Fig. 4a, the XPS signals of Co 2p in Co_3O_4 QDs/ZCS and ZCS/CoP is quite weak due to the extremely low content of Co_3O_4 QDs and CoP in composite samples. It is worth noting that the binding energies of Co 2p in Co_3O_4QDs/ZCS and ZCS/CoP exhibit a negative shift in comparison with those of Co 2p in alone Co_3O_4 QDs and CoP, which suggests that it is charges that migrate from ZCS to Co_3O_4 QDs and CoP. On the contrary, the binding energies of Zn 2p, Cd 3d and S 2p in all composite samples present remarkable positive shift in comparison with those of Zn 2p, Cd 3d and S 2p in original ZCS (Fig. 4b-d), which also indicate that it is ZCS that is the electron donor for highly-efficient photocatalytic hydrogen evolution. In addition, it also can be observed from the XPS spectrum of Zn 2p, Cd 3d and S 2p that their binding energies in O/ZCS/P bi-heterostructure cages increase more compared with those in Co_3O_4 QDs/ZCS and ZCS/CoP, which strongly reveal that Co_3O_4 QDs and CoP simultaneously transfer electrons from ZCS. Consequently, the construction of hierarchical O/ZCS/P bi-heterostructure cages can rapidly migrate charges from photo-excited ZCS, so the recombination of electron-hole pairs can be greatly inhibited, thereby the hydrogen evolution performance is enhanced seriously.

Posted on 31 Jan 2024 — The copyright holder is the author/funder. All rights reserved. No reuse without permission. — https://doi.org/10.22541/au.170669107.72727336/v1 — This is a preprint and has not been peer-reviewed. Data may be preliminary.

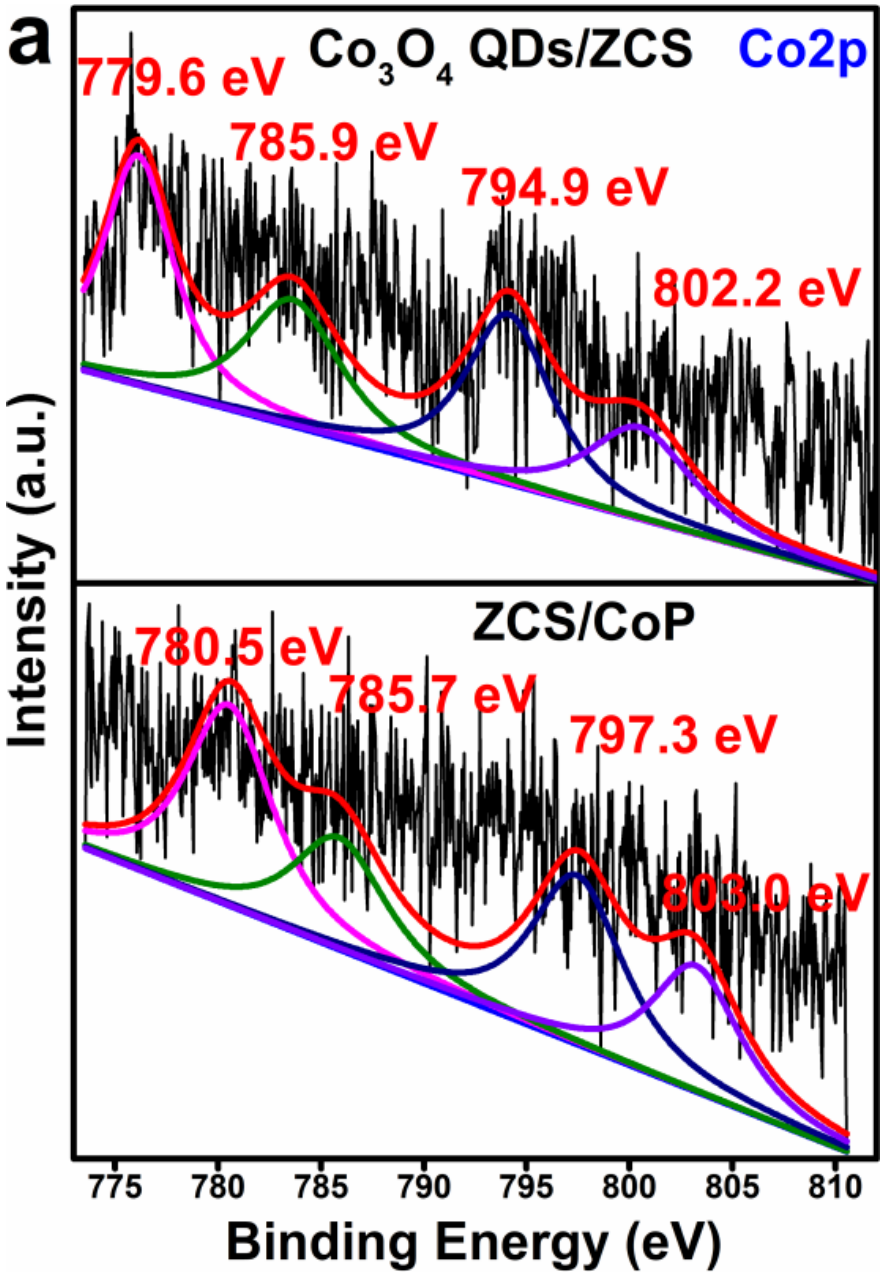

Posted on 31 Jan 2024 — The copyright holder is the author/funder. All rights reserved. No reuse without permission. — https://doi.org/10.22541/au.170669107.72727336/v1 — This is a preprint and has not been peer-reviewed. Data may be preliminary.

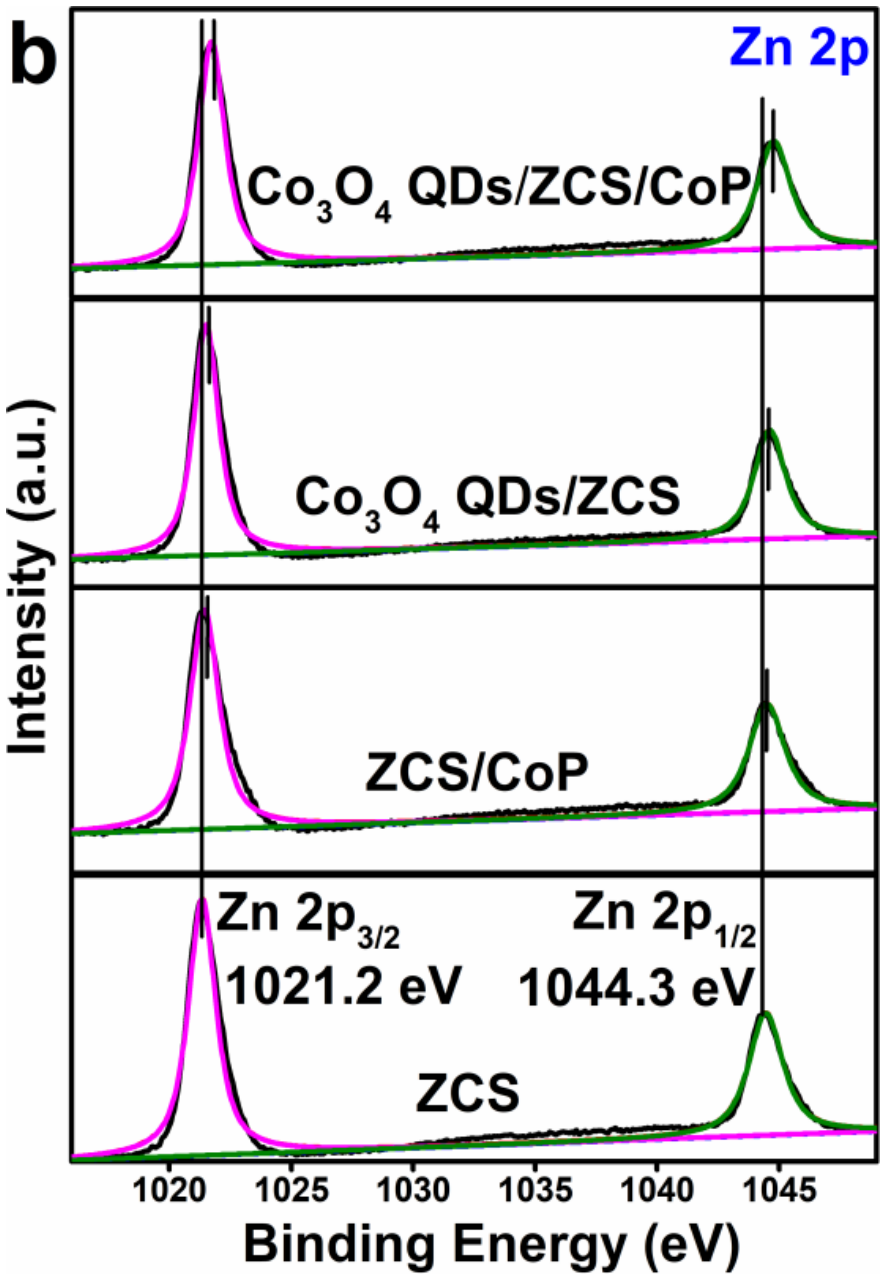

Posted on 31 Jan 2024 — The copyright holder is the author/funder. All rights reserved. No reuse without permission. — https://doi.org/10.22541/au.170669107.72727336/v1 — This is a preprint and has not been peer-reviewed. Data may be preliminary.

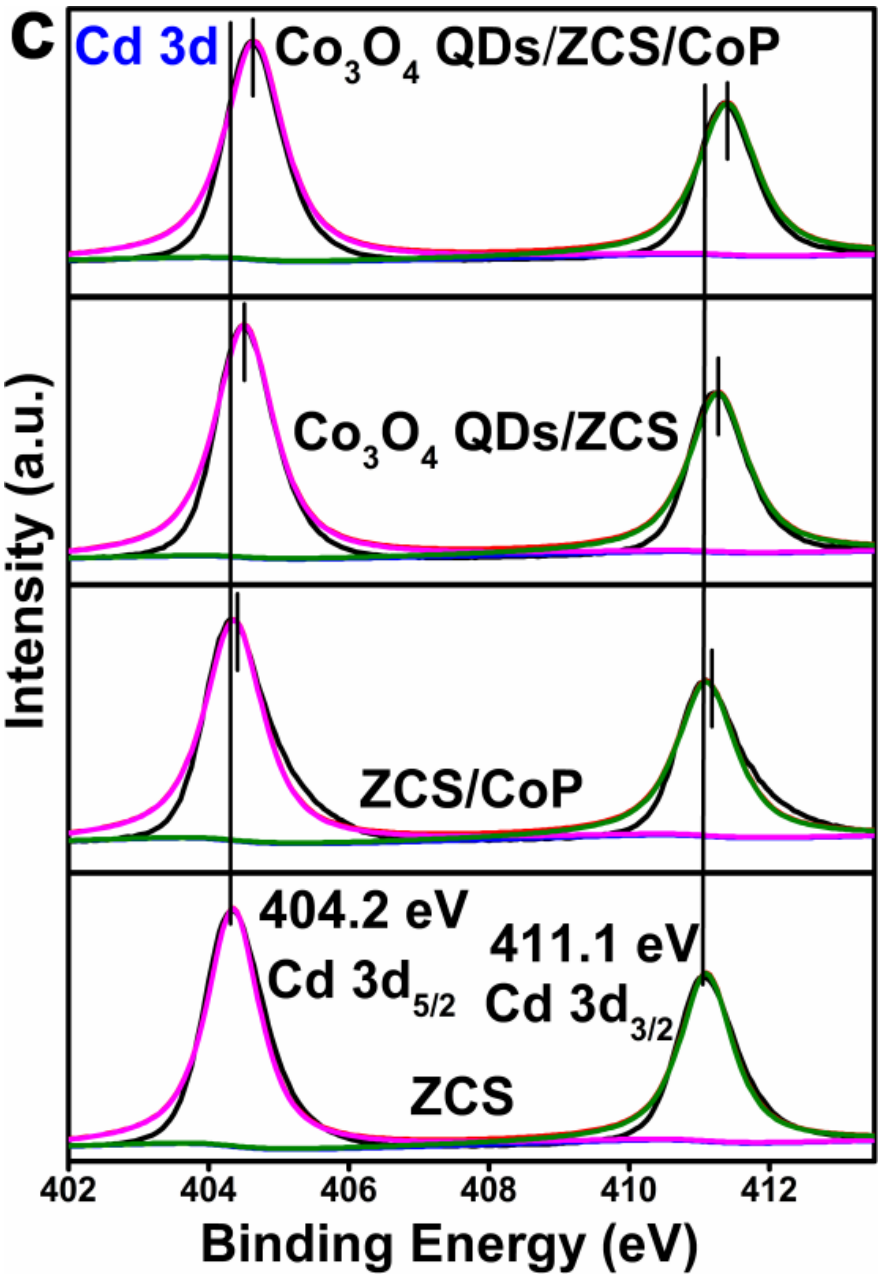

Posted on 31 Jan 2024 — The copyright holder is the author/funder. All rights reserved. No reuse without permission. — https://doi.org/10.22541/au.170669107.72727336/v1 — This is a preprint and has not been peer-reviewed. Data may be preliminary.

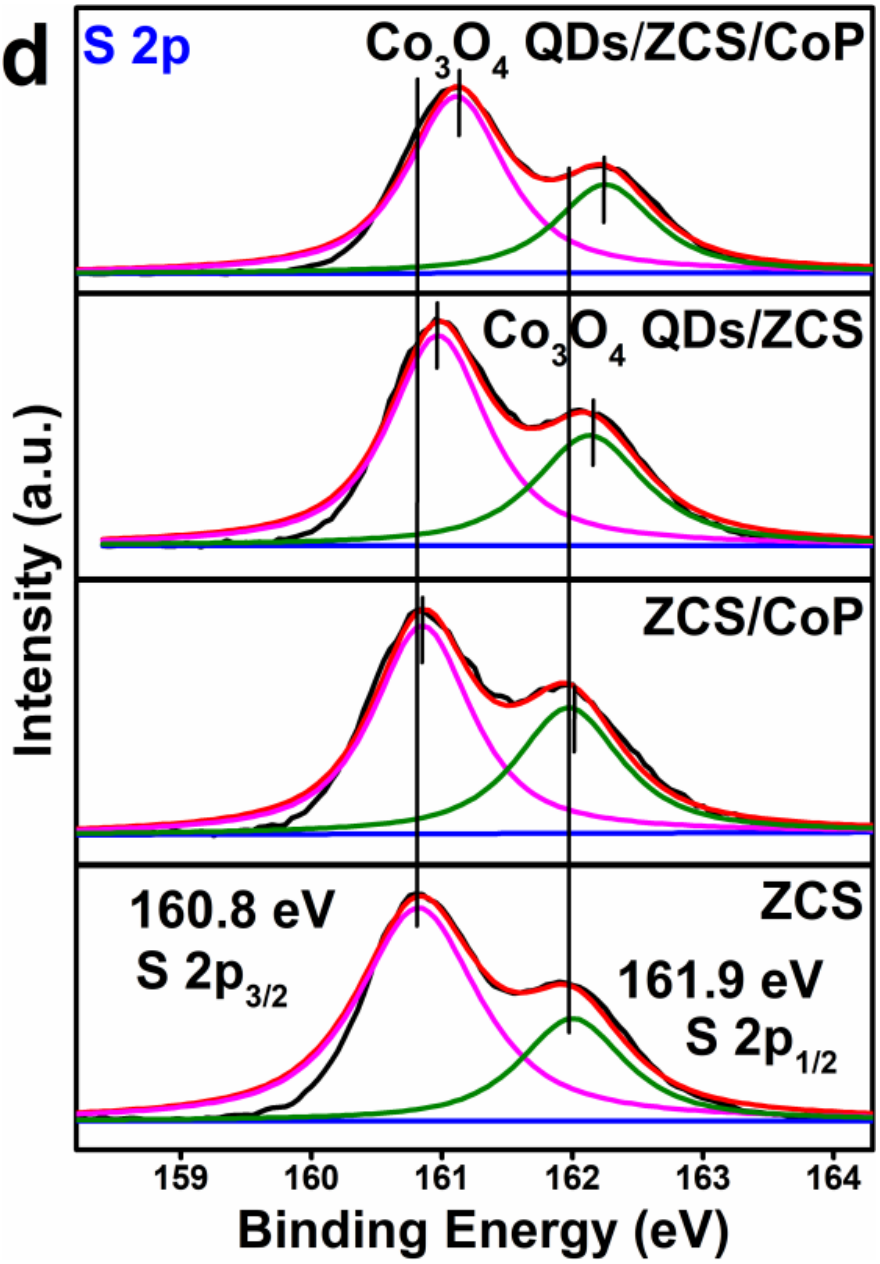

Fig. 4 XPS spectra of (a) Co 2p for Co_3O_4 QDs/ZCS and CoP/ZCS; (b) Zn 2p for ZCS, CoP/ZCS, Co_3O_4 QDs/ZCS and Co_3O_4 QDs/ZCS/CoP; (c) Cd 3d for ZCS, CoP/ZCS, Co_3O_4 QDs/ZCS and Co_3O_4 QDs/ZCS/CoP; (e) S 2p for ZCS, CoP/ZCS, Co_3O_4 QDs/ZCS and Co_3O_4 QDs/ZCS/CoP.

3.4 Brunauer-Emmett-Teller analysis

The Brunauer-Emmett-Teller (BET) specific surface area (S_{BET}) and the pore diameter distribution of ZnCdS nanoparticles, CoP polyhedrons, Co_3O_4 QDs and bi-heterostructured O/ZCS/P-3 cages were analyzed by N_2adsorption-desorption measurements as displayed in Fig. 5. The type IV isotherms with type H3 hysteresis loops in Fig. 5a and the pore diameter distribution curves in Fig. 5b indicate the presence of mesoporous structure in the four as-synthesized photocatalysts, which will facilitate the mass transfer for heterogeneous catalysis [41]. And the average pore size of ZnCdS nanoparticles, CoP polyhedrons, Co_3O_4QDs

and O/ZCS/P-3 is 20, 18, 4 and 22 nm, respectively. In comparison with CoP polyhedrons and Co_3O_4 QDs, ZnCdS nanoparticles possess a relatively small surface area of 30 $m^2 \cdot g^{-1}$ owing to its relatively larger density. However, an enlarged BET surface area of 37 $m^2 \cdot g^{-1}$ for hierarchical O/ZCS/P-3 bi-heterostructure cages was gained because of the integration of both CoP (79 $m^2 \cdot g^{-1}$) polyhedrons and Co_3O_4 QDs (178 $m^2 \cdot g^{-1}$) with ZnCdS nanoparticles, which ensures more active sites for photocatalytic hydrogen evolution reaction.

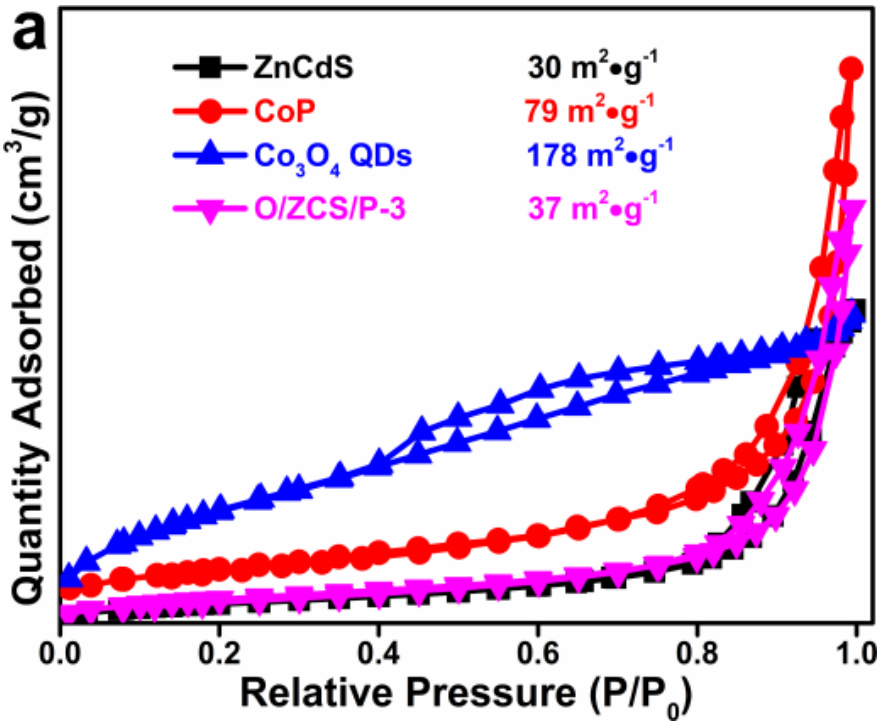

Posted on 31 Jan 2024 — The copyright holder is the author/funder. All rights reserved. No reuse without permission. — https://doi.org/10.22541/au.170669107.72727336/v1 — This is a preprint and has not been peer-reviewed. Data may be preliminary.

Posted on 31 Jan 2024 — The copyright holder is the author/funder. All rights reserved. No reuse without permission. — https://doi.org/10.22541/au.170669107.72727336/v1 — This is a preprint and has not been peer-reviewed. Data may be preliminary.

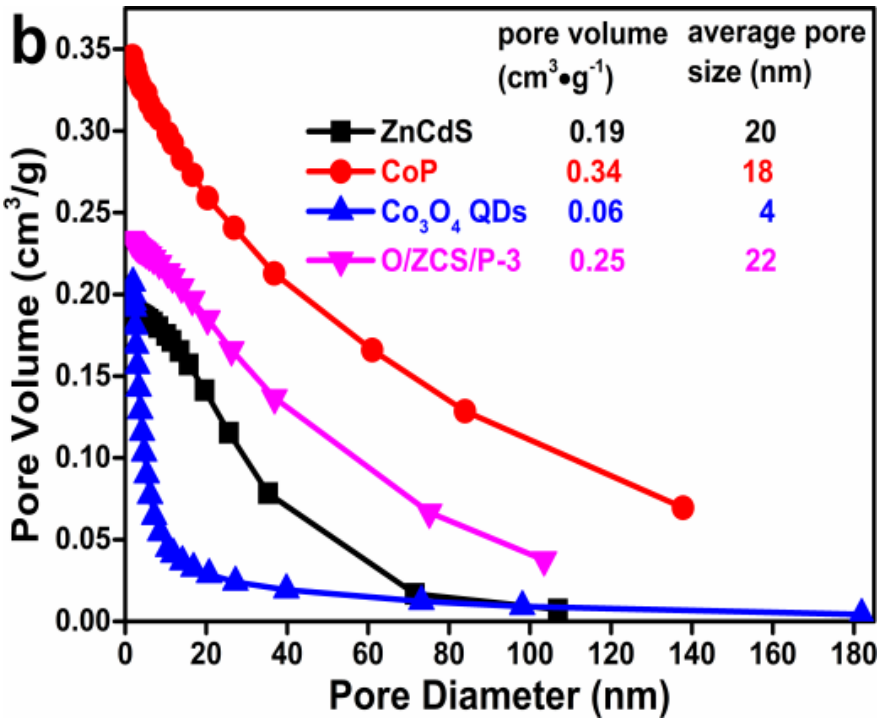

Fig. 5 (a) N_2 adsorption-desorption and (b) pore diameter distribution curves of ZnCdS, CoP, Co_3O_4 QDs and O/ZCS/P-3.

3.5 UV-vis DRS analysis

As observed in Fig. 6, the optical properties of pristine ZnCdS nanoparticles, CoP polyhedrons, Co_3O_4 QDs are investigated by the UV-vis diffuse reflectance spectra (UV-vis DRS). Obviously, UV-vis DRS depict the fact that the three samples manifest strong visible light absorption. And original ZnCdS nanoparticles exhibit a light absorption with an edge of about 560 nm, meaning the significant semiconductor characteristics. However, the CoP polyhedrons and Co_3O_4 QDs exhibit an intense light absorption from 300 to 800 nm, implying their semi-metallic nature nature [42,43]. In fact, TMPs have been proved to have semi-metallic nature and high electrical conductivity. QDs with narrow emission bandwidth are confined three-dimensionally. Thus, CoP and Co_3O_4QDs can serve as electron sink to greatly promote the separation efficiency of charges from ZnCdS and fundamentally inhibit the recombination of photo-excited carriers, so as to lead to highly-efficient hydrogen evolution rate.

Posted on 31 Jan 2024 — The copyright holder is the author/funder. All rights reserved. No reuse without permission. — https://doi.org/10.22541/au.170669107.72727336/v1 — This is a preprint and has not been peer-reviewed. Data may be preliminary.

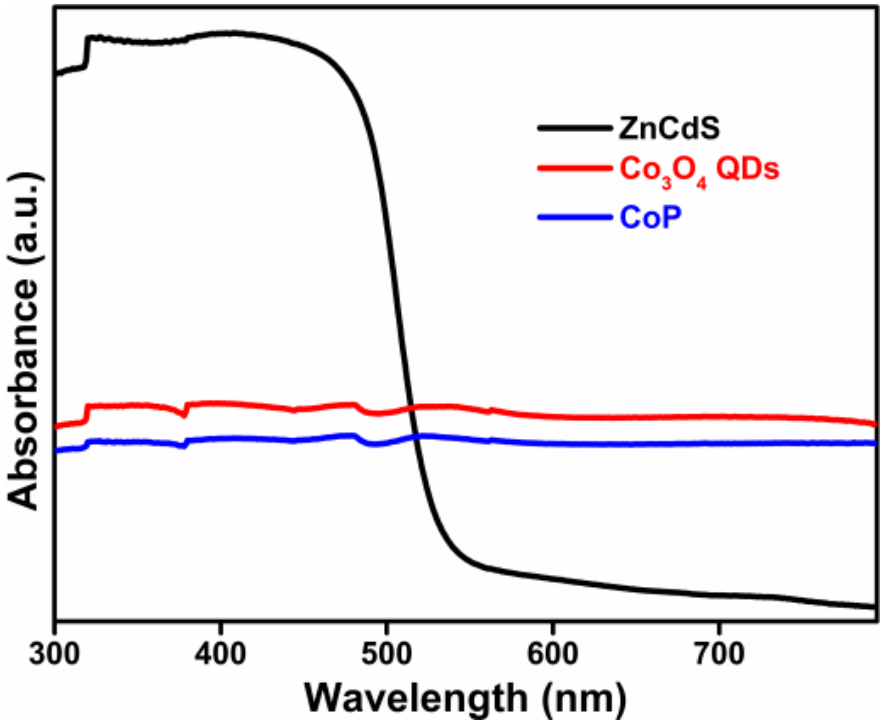

Fig.6. (a) UV-vis diffusion reflectance spectra (UV-vis DRS) of ZnCdS, Co_3O_4 QDs and CoP.

3.6 Photocatalytic H_2 evolution activity measurements

Fig. 7a depicts the photocatalytic hydrogen evolution performance of different samples under visible light irradiation (λ [?] 400 nm) with lactic acid (LA) as the hole scavenger. The original ZnCdS nanoparticles are visibly active to catalyze the splitting of water under 5 W LED light irradiation, giving a H_2-evolving rate of 8.2 mmol h^{-1} g^{-1}. However, after coupling 0.5 wt.% CoP polyhedron or 0.5 wt.% Co_3O_4 QDs with ZnCdS nanoparticles, the as-obtained ZCS/CoP and ZCS/Co_3O_4 QDs hybrids show an improved hydrogen evolution activity, which manifests that the introduction of both CoP polyhedron and Co_3O_4 QDs can accelerate the separation and migration of photo-excited charges from ZCS. More importantly, while 0.5 wt.% CoP polyhedron and 0.5 wt.% Co_3O_4 QDs were introduced concurrently, the constructed hierarchical CoP/ZnCdS/Co_3O_4QDs (800>40>4.5 nm) bi-heterostructure cages exhibits more high-performance photocatalytic hydrogen production, which strongly indicates that the parallel pathways of electron migration was successfully established for more rapider charge transport. Fig. 7b shows the comparison of hydrogen evolution rate of ZCS/CoP with different wt.% of CoP polyhedron. It can be clearly observed that ZCS/CoP with 1.5 wt.% CoP exhibits higher hydrogen generation rate (12.4 mmol h^{-1} g^{-1}) which is 1.5 times that of pristine ZCS, again demonstrating the significant role of CoP for promoting the hydrogen evolution activity of ZCS. Fig. 7c displays the hydrogen production activities after assembling different content of Co_3O_4QDs on ZCS/CoP-3. As observed, the O/ZCS/P-3 with 1.5 wt.% Co_3O_4 QDs exhibits the highest photocatalytic hydrogen evolution property (24.2 mmol h^{-1} g^{-1}) under 5 W LED light irradiation, which is about 2.9 times that of original ZCS. Further, O/ZCS/P-3 possesses more prominent hydrogen generation performance under 300 W Xe lamp irradiation close to sunlight (Fig. 7d), and a large number of bubbles can be clearly observed in a closed reaction vessel as shown in Fig. 7g, which seriously reveal the ultrahigh photocatalytic performance of the hierarchical O/ZCS/P-3 bi-heterostructure cages for hydrogen evolution. In order to more intuitively evaluate the photocatalytic hydrogen evolution rate of the bi-heterostructured O/ZCS/P-3 cages, the reaction vessel was equipped with H_2-collection-device (HCD). Dynamic bubbles in hydrogen evolution reaction is provided in a separate document (H_2-evolution video). While the hydrogen evolution reaction

proceed for 0 h, the HCD of easy expansion is downcast. After 5 h, it was obviously bulging. However, it's completely propped up after 10 h. Both lots of bubbles and the rapid bulging of elastic HCD indicate the ultrahigh photocatalytic hydrogen evolution performance of the as-constructed O/ZCS/P-3 bi-heterostructure cages. Additionally, the purity of evolved H_2 also was tested via ignition experiment, bright flame means the high purity of $H_2$from O/ZCS/P-3 driven water splitting under visible light irradiation. Undoubtedly, the hierarchical O/ZCS/P-3 bi-heterostructure cages should be one of the world-level photocatalysts for efficient H_2 evolution up to now. The hydrogen generation performance of O/ZCS/P-3 under different wavelength was carried out (1 h), the results are shown in Fig. 7e. Obviously, the decrease of photocatalytic hydrogen evolution rate is drastic at the wavelengths greater than 500 nm, which indicates that the water splitting reaction for H_2 evolution is indeed titillated by the light excitation of the O/ZCS/P-3 photocatalyst. And the H_2 evolution rate of O/ZCS/P-3 is the fastest at the wavelength of 450 nm. Furthermore, it also can be observed from Fig. 7f that the hierarchical O/ZCS/P-3 bi-heterostructure photocatalyst not only exhibits ultrahigh H_2 production properties but also very good stability, which are mainly contributed to the construction of the two efficient parallel approaches applied to the fast migration of photo-induced charges in the architecture of hierarchical O/ZCS/P-3 bi-heterostructure cages.

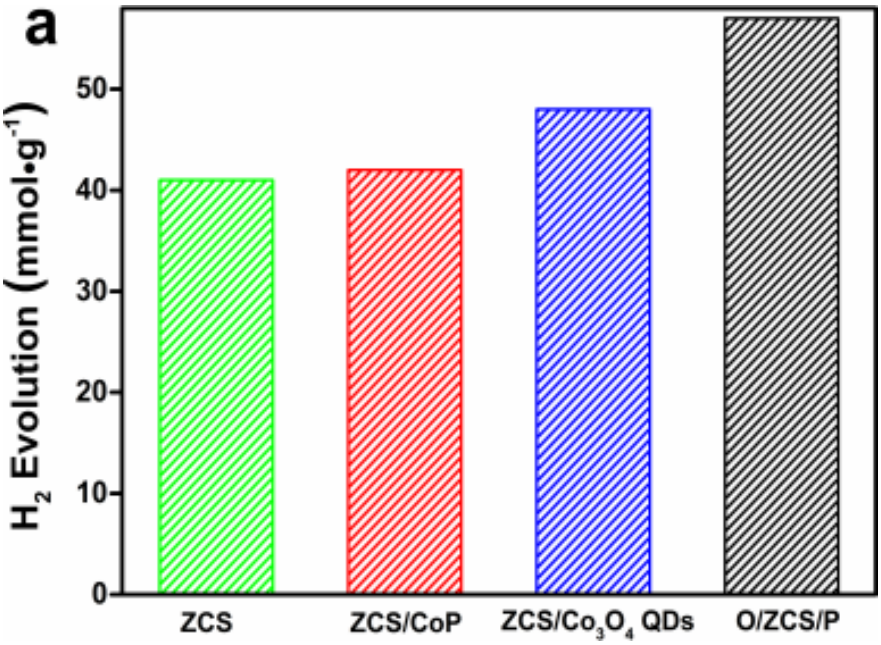

Posted on 31 Jan 2024 — The copyright holder is the author/funder. All rights reserved. No reuse without permission. — https://doi.org/10.22541/au.170669107.72727336/v1 — This is a preprint and has not been peer-reviewed. Data may be preliminary.

Posted on 31 Jan 2024 — The copyright holder is the author/funder. All rights reserved. No reuse without permission. — https://doi.org/10.22541/au.170669107.72727336/v1 — This is a preprint and has not been peer-reviewed. Data may be preliminary.

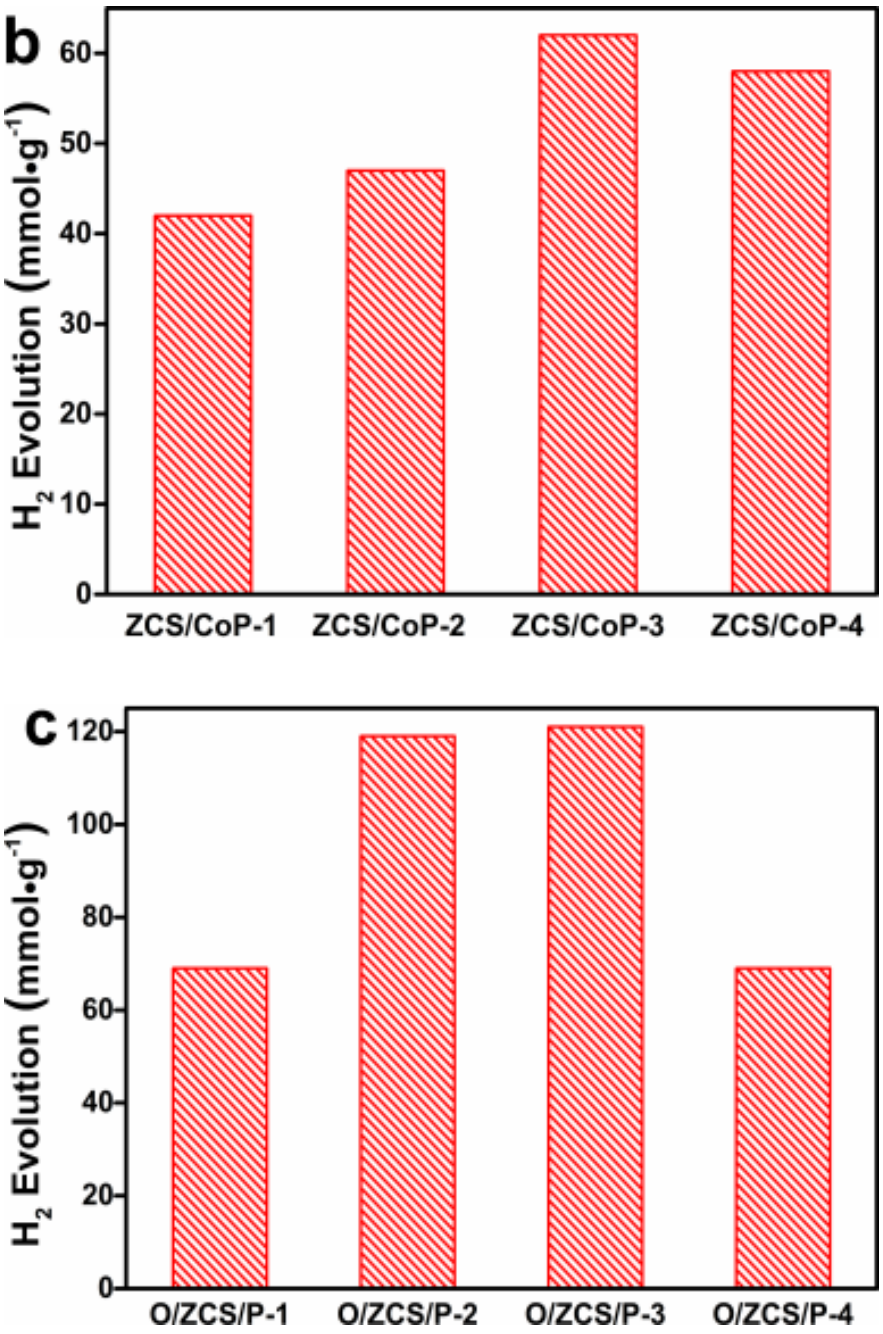

Posted on 31 Jan 2024 — The copyright holder is the author/funder. All rights reserved. No reuse without permission. — https://doi.org/10.22541/au.170669107.72727336/v1 — This is a preprint and has not been peer-reviewed. Data may be preliminary.

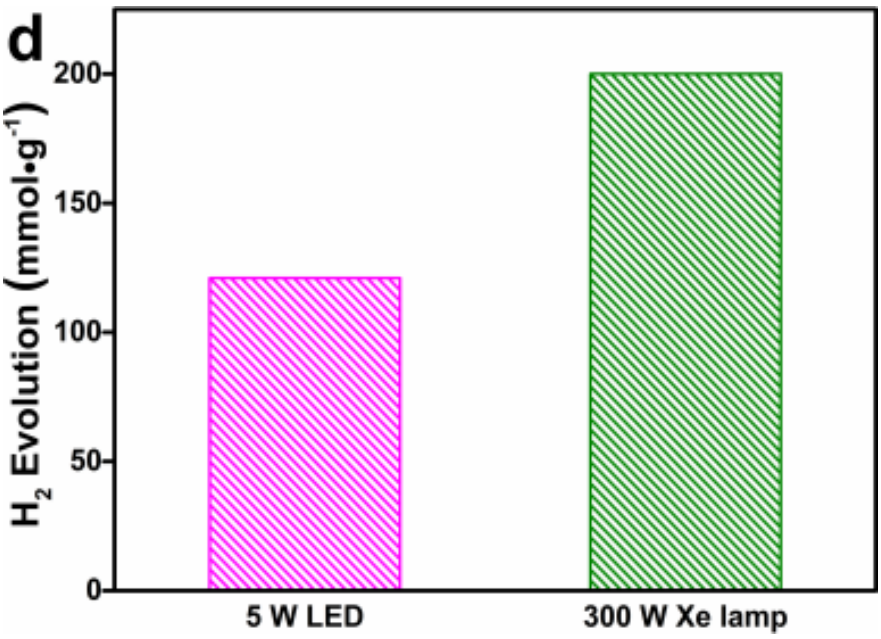

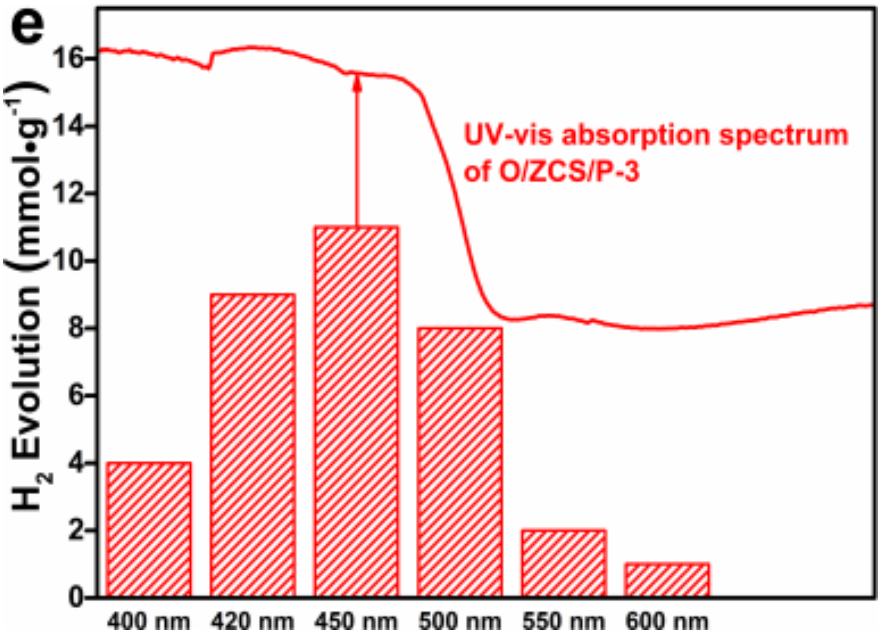

Posted on 31 Jan 2024 — The copyright holder is the author/funder. All rights reserved. No reuse without permission. — https://doi.org/10.22541/au.170669107.72727336/v1 — This is a preprint and has not been peer-reviewed. Data may be preliminary.

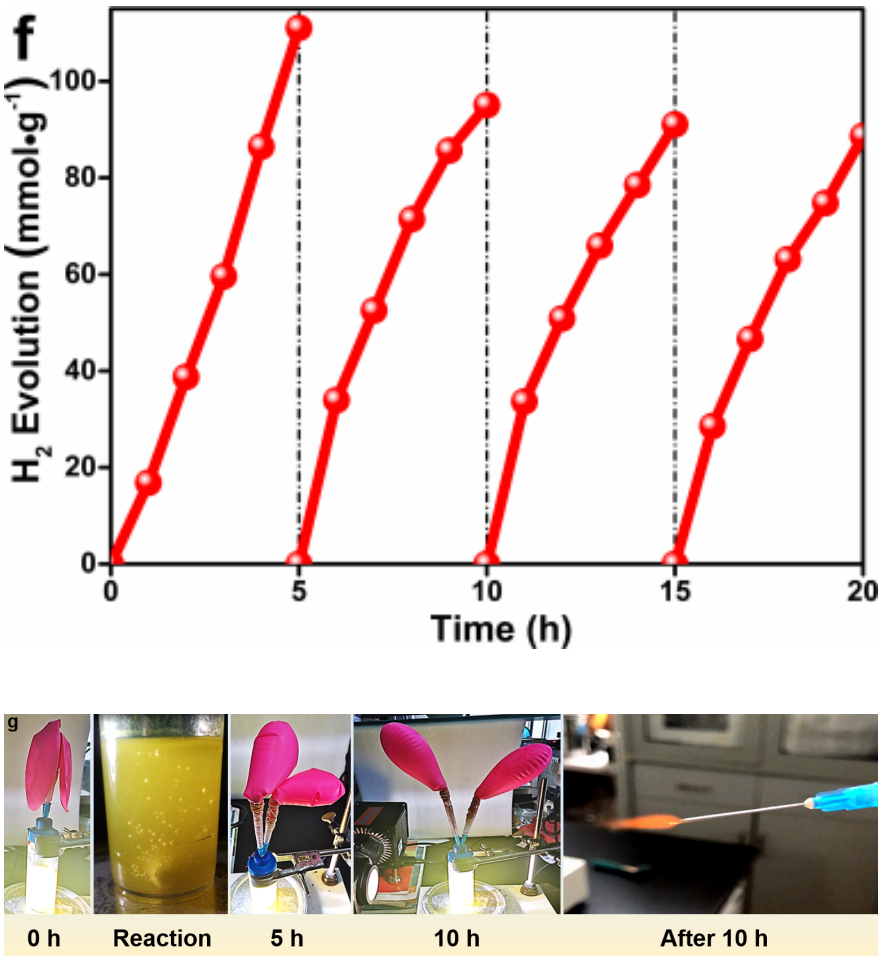

Fig. 7 (a) H_2 evolution activity of ZCS, ZCS/CoP, ZCS/Co_3O_4 QDs and O/ZCS/P; (b) H_2 evolution activity of ZCS/CoP-x; (c) H_2 evolution activity of O/ZCS/P-x; (d) H_2 evolution activity of O/ZCS/P-3 under different light sources; (e) H_2 evolution activity of O/ZCS/P-3 under different wavelength (1 h); (f) Photocatalytic H_2evolution stability testing of O/ZCS/P-3.

3.7 Photophysical and electrochemical properties

In order to further gain some insights into the excellent performance of bi-heterostructured O/ZCS/P-3 cages, various electro-/photo-chemical characterizations are carried out as displayed in Fig. 8. The most accelerated charge migration kinetics in O/ZCS/P-3 is clearly reflected by the significantly increased photocurrent response as shown in Fig. 8a. Moreover, electrochemical impedance spectra (EIS) exhibit that ITO/O/ZCS/P-3 electrode possesses a smaller high-frequency semicircle compared with other three electrodes (Fig. 8b), indicating a lower electron-transport resistance in the O/ZCS/P-3 material that ensures the faster charge migration. On the other hand, steady-state photoluminescence (PL) quenching reveals the most inhibited recombination of light-excited electron-hole pairs in O/ZCS/P-3 (Fig. 8c). Furthermore, time-resolved photoluminescence (TRPL) spectroscopy is applied to investigate the charge carrier dynamics of the as-prepared semiconductors (Fig. 8d). The decay kinetics of O/ZCS/P-3 exhibits shorter average lifetime (1.62 ns) in comparison with those of ZCS (1.78 ns), ZCS/CoP (1.75 ns) and ZCS/ Co_3O_4 QDs (1.70 ns), which signifies the O/ZCS/P-3 can faster promote the separation of photo-induced charge carriers. These results verify the faster separation and migration of light-excited charges in O/ZCS/P-3, thus leading to the high-performance H_2 evolution.

Posted on 31 Jan 2024 — The copyright holder is the author/funder. All rights reserved. No reuse without permission. — https://doi.org/10.22541/au.170669107.72727336/v1 — This is a preprint and has not been peer-reviewed. Data may be preliminary.

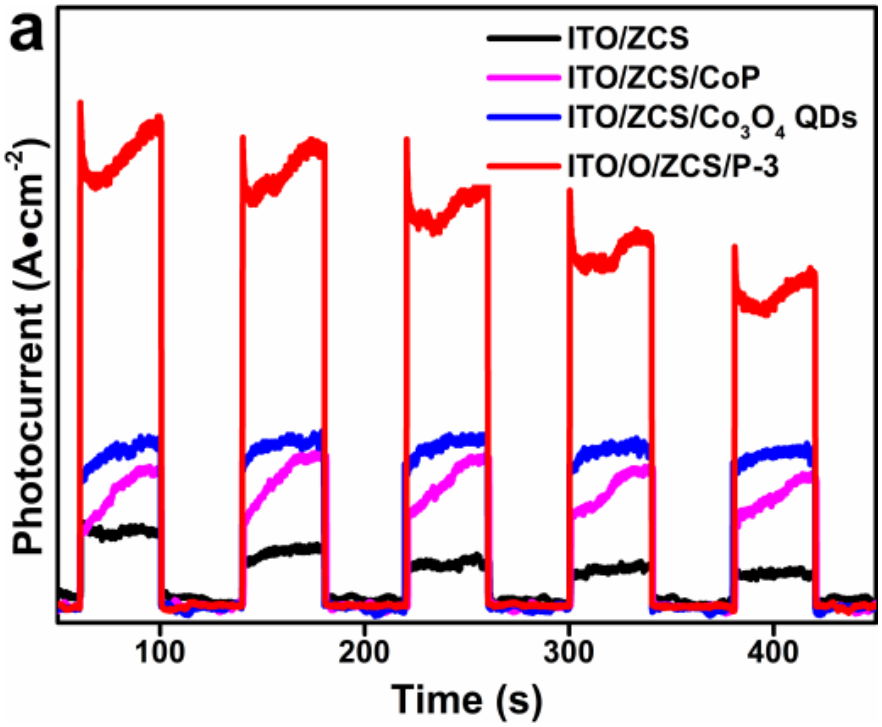

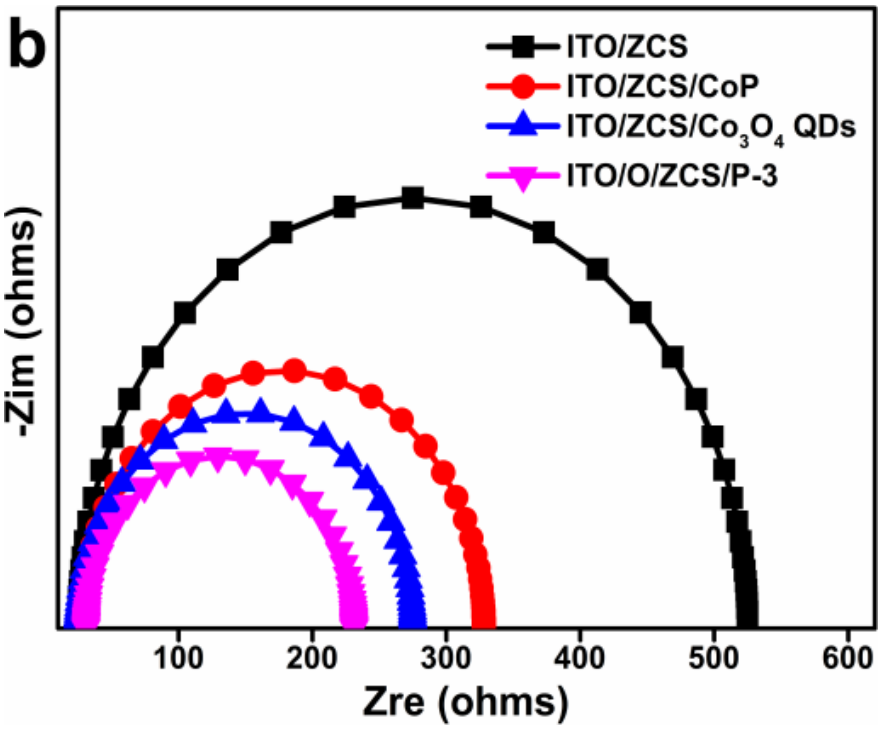

Posted on 31 Jan 2024 — The copyright holder is the author/funder. All rights reserved. No reuse without permission. — https://doi.org/10.22541/au.170669107.72727336/v1 — This is a preprint and has not been peer-reviewed. Data may be preliminary.

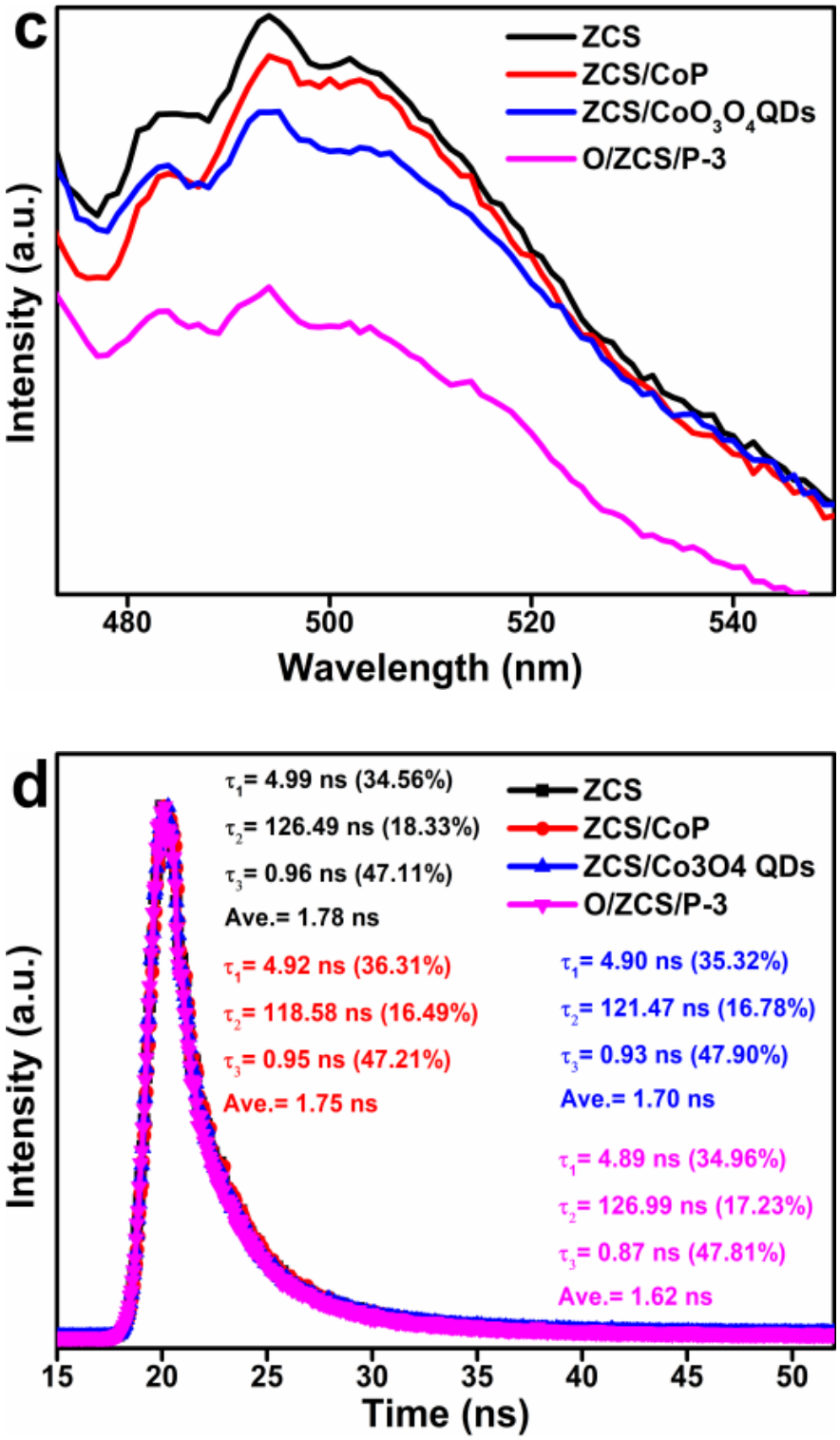

Fig. 8 (a) Time-photocurrent response and (b) EIS curves of ITO/ZCS, ITO/ZCS/CoP, ITO/ZCS/Co_3O_4 QDs and ITO/O/ZCS/P-3 electrodes; (c) Steady-state PL spectra and (d) Time-resolved PL emission decay curves of ZCS, ZCS/CoP, ZCS/Co_3O_4 QDs, and O/ZCS/P-3.

Posted on 31 Jan 2024 — The copyright holder is the author/funder. All rights reserved. No reuse without permission. — https://doi.org/10.22541/au.170669107.72727336/v1 — This is a preprint and has not been peer-reviewed. Data may be preliminary.

3.8 Photocatalytic H_2 evolution mechanism

Based on the above experimental results, the H_2evolution mechanism of the hierarchical CoP/ZnCdS/Co_3O_4 QDs bi-heterostructure cages as a photocatalyst exhibiting ultrahigh hydrogen evolution activity is depicted as shown in Fig. 9. Under visible light irradiation, ZnCdS solid solution being inherently active to splitting of water is excited to generate electrons and holes, and the produced charges are rapidly captured and transferred by the excellent-performance CoP and Co_3O_4 QDs while the holes on valence band of ZnCdS react with LA as the sacrificial reagent, which lead to that the recombination of electron-hole pairs is greatly inhibited, thereby the high-performance photocatalytic hydrogen evolution come. In short, the construction of the bi-heterostructured cages in CoP/ZnCdS/Co_3O_4 QDs develops the two parallel pathways applied to the rapid electron transport, resulting in the serious improvement of the utilization efficiency of photo-induced charges on conduction band of ZnCdS for hydrogen evolution.

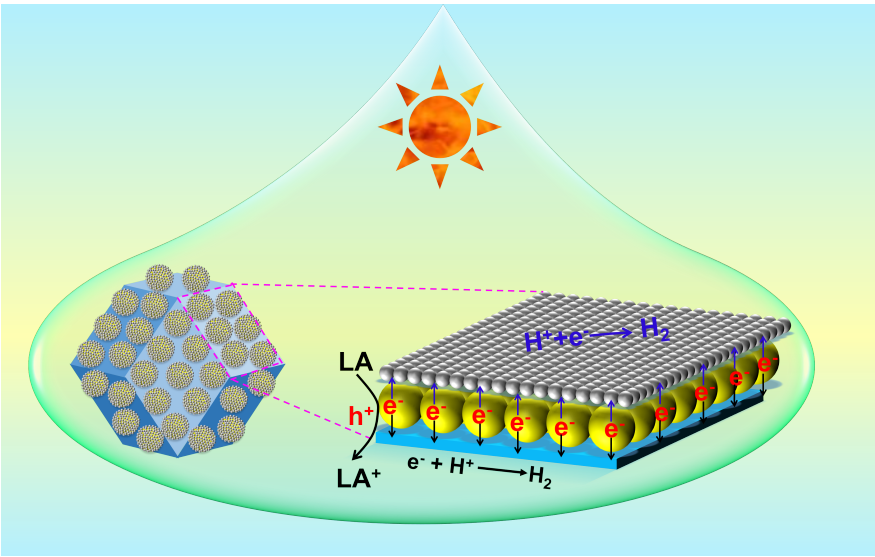

Fig. 9 Internal migration mechanism of electrons in CoP/ZnCdS/Co_3O_4 QDs bi-heterostructures.

4. Conclusion

Summarily, hierarchical CoP/ZnCdS/Co_3O_4QDs bi-heterostructure cages was constructed by integrating about 800 nm CoP polyhedron, 40 nm ZnCdS nanoparticles and 4.5 nm Co_3O_4 QDs into all-in-one as an ultrahigh-performance photocatalyst for visible-light-driven water splitting. What's more, the development of the two parallel electron-transfer pathways in the bi-heterostructured CoP/ZnCdS/Co_3O_4 QDs cages makes photo-excited charges in ZnCdS be used seriously to the hydrogen evolution reaction. Undoubtedly, both semi-metallic CoP and three-dimensionally confined Co_3O_4 QDs as electron traps efficiently separated and transferred charges in photocatalytic water-splitting reaction. Besides, the CoP/ZnCdS/Co_3O_4 QDs photocatalyst not only exhibited high-efficiency H_2-evolution but also favorable recycling stability.

Author contributions

Yanbing Li and Pengfei Zhu conceived and designed the experiments; Yanbing Li and Zhiling Jin performed the experiments; Noritatsu Tsubaki and Zhiling Jin contributed reagents/materials and analysis tools; and Yanbing Li wrote the paper.

Conflicts of interest

The authors declare that they have no competing interests.

Acknowledgements

Posted on 31 Jan 2024 — The copyright holder is the author/funder. All rights reserved. No reuse without permission. — https://doi.org/10.22541/au.170669107.72727336/v1 — This is a preprint and has not been peer-reviewed. Data may be preliminary.

This work was financially supported by the Chinese National Natural Science Foundation (22062001) and the innovation team of clean energy and green chemical engineering, State Ethnic Affairs Commission.

References

1. T. Banerjee, K. Gottschling, G. Savasci, C. Ochsenfeld, B. V. Lotsch, H_2 evolution with covalent organic framework photocatalysts, ACS Energy Lett. 3 (2018) 400-409.
2. C. Bie, H. Yu, Bei Cheng, W. Ho, J. J. Fan, J. G. Yu, Design, fabrication, and mechanism of nitrogen-doped graphene-based photocatalyst, Adv. Mater. 33 (2021) 2003521.
3. Q. L. Xu, B. C. Zhu, B. Cheng, J. G. Yu, M. H. Zhou, W. Ho, Photocatalytic H_2 evolution on graphdiyne/g-C_3N_4 hybrid nanocomposites, Appl. Catal. B 255 (2019) 117770.
4. D. D. Ren, Z. Z. Liang, Y. H. Ng, P. Zhang, Q. J. Xiang, X. Li, Strongly coupled 2D-2D nanojunctions between P-doped Ni_2S (Ni_2SP) cocatalysts and CdS nanosheets for efficient photocatalytic H_2 evolution, Chem. Eng. J. 390 (2020) 124496.
5. Q. Z. Wang, J. J. He, Y. B. Shi, S. L. Zhang, T. J. Niu, H. D. She, Y. P. Bi, Z. Q. Lei, Synthesis of MFe_2O_4(M = Ni, Co)/$BiVO_4$ film for photolectrochemical hydrogen production activity, Appl. Catal. B 214 (2017) 158-167.
6. R. C. Shen, Y. N. Ding, S. B. Li, P. Zhang, Q. J. Xiang, Y. H. Ng, X. Li, Constructing low-cost Ni_3C/twin-crystal $Zn_{0.5}Cd_{0.5}S$ heterojunction/homojunction nanohybrids for efficient photocatalytic H_2 evolution, Chinese J. Catal. 42 (2021) 25-36.
7. J. L. Yang, Y. L. He, H. Ren, H. L. Zhong, J. S. Lin, W. M. Yang, M. D. Li, Z. L. Yang, H. Zhang, Z. Q. Tian, J. F. Li, Boosting photocatalytic hydrogen evolution reaction using dual plasmonic antennas. ACS Catal. 11 (2021) 5047-5053.
8. M. Y. Zhang, Q. Y. Hu, K. W. Ma, Y. Ding, C. Li, Pyroelectric effect in CdS nanorods decorated with a molecular Co-catalyst for hydrogen evolution, Nano Energy 73 (2020) 104810.
9. Y. X. Li, P. Han, Y. L. Hou, S. Q. Peng, X. J. Kuang, Oriented $Zn_mIn_2S_{m+3}$@In_2S_3heterojunction with hierarchical structure for efficient photocatalytic hydrogen evolution, Appl. Catal. B 244 (2019) 604-611.
10. X. W. Jiang, H. S. Gong, Q. W. Liu, M. X. Song, C. J. Huang, In situ construction of NiSe/$Mn_{0.5}Cd_{0.5}S$ composites for enhanced photocatalytic hydrogen production under visible light, Appl. Catal. B 268 (2020) 118439.
11. C. Xue, H. Li, H. An, B. L. Yang, J. J. Wei, G. D. Yang, NiS_x quantum dots accelerate electron transfer in $Cd_{0.8}Zn_{0.2}S$ photocatalytic system via an rGO nanosheet "bridge" toward visible-light-driven hydrogen evolution, ACS Catal. 8 (2018) 1532-1545.
12. X. Liu, X. Q. Li, L. X. Qin, J. Mu, S. Z. Kang, Dramatic enhancement of the photocatalytic activity of $Cd_{0.5}Zn_{0.5}S$ nanosheets via phosphorization calcination for visible-light-driven H_2 evolution, J. Mater. Chem. A 5 (2017) 14682-14688.
13. S. N. Guo, Y. L. Min, J. C. Fan, Q. J. Xu, Stabilizing and improving solar H_2 generation from $Zn_{0.5}Cd_{0.5}S$ nanorods@MoS_2/RGO hybrids via dual charge transfer pathways, ACS Appl. Mate. Interfaces 8 (2016) 2928-2934.
14. D. L. Huang, M. Wen, C. Y. Zhou, Z. H. Li, M. Cheng, S. Chen, W. J. Xue, L. Lei, Y. Yang, W. P. Xiong, W. J. Wang, $Zn_xCd_{1-x}S$ based materials for photocatalytic hydrogen evolution, pollutants degradation and carbon dioxide reduction, Appl. Catal. B 267 (2020) 118651.
15. M. L. Huang, X. Y. Luo, Z. Z. Ai, Y. L. Li, K. Zhang, Y. L. Shao, B. B. Huang, Y. Z. Wu, X. P. Hao, Band structure-controlled $Zn_{1-x}Cd_xS$ solid solution for photocatalytic hydrogen production improvement via appropriately enhancing oxidation capacity, Solar RRL 5 (2021) 2000685.
16. Q. Li, H. Meng, P. Zhou, Y. Q. Zheng, J. Wang, J. G. Yu, J. R. Gong, $Zn_{1-x}Cd_xS$ solid solutions with controlled bandgap and enhanced visible-light photocatalytic H_2-production activity, ACS Catal. 3 (2013) 882-889.
17. Y. B. Li, Z. L. Jin, H. Liu, H. Y. Wang, Y. P. Zhang, G. R. Wang, Unique photocatalytic activities of transition metal phosphide for hydrogen evolution, J. Colloid and Interface Sci. 5451 (201) 287-299.
18. A. Agarwal, B. R. Sankapal, Metal phosphides: topical advances in the design of supercapacitors, J.

Posted on 31 Jan 2024 — The copyright holder is the author/funder. All rights reserved. No reuse without permission. — https://doi.org/10.22541/au.170669107.72727336/v1 — This is a preprint and has not been peer-reviewed. Data may be preliminary.

Mater. Chem. A 9 (202) 20241-20276.
19. X. Li, A. M. Elshahawy, C. Guan, J. Wang, Metal phosphides and phosphates-based electrodes for electrochemical supercapacitors, Small 13 (2017) 1701530.
20. S. T. Oyama, T. Gott, H. Y. Zhao, Y. K. Lee, Transition metal phosphide hydroprocessing catalysts: A review, Catal. Today 143 (2009) 94-10.
21. H. N. Ma, J. He, D. B. Xiong, J. S. Wu, Q. Q. Li, V. Dravid, Y. F. Zhao, Nickel cobalt hydroxide@reduced graphene oxide hybrid nanolayers for high performance asymmetric supercapacitors with remarkable cycling stability, ACS Appl. Mater. Interfaces 8 (2016) 1992-2000.
22. X. Wang, H. M. Kim, Y. Xiao, Y. K. Sun, Nanostructured metal phosphide-based materials for electrochemical energy storage, J. Mater. Chem. A 4 (2016) 14915-14931.
23. Y. M. Shia, B. Zhang, Recent advances in transition metal phosphide nanomaterials: synthesis and applications in hydrogen evolution reaction, Chem. Soc. Rev. 45 (2016) 1529-1541.
24. P. Liu, J. A. Rodriguez, Catalysts for hydrogen evolution from the [NiFe] hydrogenase to the Ni_2P (001) surface: The importance of ensemble effect, J. Ame. Chem. Soc. 127 (2005) 14871-14878.
25. Y. B. Li, Z. L. Jin, T. S. Zhao, Performance of ZIF-67-derived fold polyhedrons for enhanced photocatalytic hydrogen evolution, Chem. Eng. J. 382 (2020) 123051.
26. S. Cao, Y. Chen, C. J. Wang, X. J. Lv, W. F. Fu, Spectacular photocatalytic hydrogen evolution usingmetal-phosphide/CdS hybrid catalysts under sunlight irradiation, Chem. Commun. 51 (2015) 8708-8711.
27. J. Y. Kim, O. Voznyy, D. Zhitomirsky, E. H. Sargent, 25th anniversary article: Colloidal quantum dot materials and devices: A quarter-century of advances, Adv. Mater. 25 (2013) 4986-5010.
28. A. J. Nozik, M. C. Beard, J. M. Luther, M. Law, R. J. Ellingson, J. C. Johnson, Semiconductor quantum dots and quantum dot arrays and applications of multiple exciton generation to third-generation photovoltaic solar cells, Chem. Rev. 110 (2010) 6873-6890.
29. H. Moon, C. Lee, W. Lee, J. Kim, H. Chae, Stability of quantum dots, quantum dot films, and quantum dot light-emitting diodes for display applications, Adv. Mater. 31 (2019) 1804294.
30. N. Shi, W. Cheng, H. Zhou, T. X. Fan, M. Niederberger, Facile synthesis of monodisperse Co_3O_4quantum dots with efficient oxygen evolution activity, Chem. Commun. 51 (2015) 1338-1340.
31. B. Luo, R. Song, J. F. Geng, X. H. Liu, D. W. Jing, M. L. Wang, C. Cheng, Towards the prominent cocatalytic effect of ultra-small CoP particles anchored on g-C_3N_4nanosheets for visible light driven photocatalytic H_2production, Appl. Catal. B 256 (2019) 117819.
32. X. Q. Hao, D. Z. Xiang, Z. L. Jin, Amorphous Co_3O_4 quantum dots hybridizing with 3D hexagonal CdS single crystals to construct a 0D/3D p-n heterojunction for a highly efficient photocatalytic H_2 evolution, Dalton Trans. 50 (2021) 10501-10514.
33. Y. N. Guo, J. Tang, H. Y. Qian, Z. L. Wang, Y. Yamauchi, One-pot synthesis of zeolitic imidazolate framework 67-derived hollow Co_3S_4@MoS_2heterostructures as efficient bifunctional catalysts, Chem. Mater. 29 (2017) 5566-5573.
34. H. M. Gong, X. Q. Hao, Z. L. Jin, Q. X. Ma, WP modified S-scheme $Zn_{0.5}Cd_{0.5}S/WO_3$ for efficient photocatalytic hydrogen production, New J. Chem. 43 (2019) 19159.
35. H. S. Gong, Z. Li, Z. H. Chen, Q. W. Liu, M. X. Song, C. J. Huang, NiSe/$Cd_{0.5}Zn_{0.5}S$ composite nanoparticles for use in p-n heterojunction-based photocatalysts for solar energy harvesting, ACS Appl. Nano Mater. 3 (2020) 3665-3674.
36. P. F. Wang, T. F. Wu, Y. H. Ao, C. Wang, Fabrication of noble-metal-free CdS nanorods-carbon layer-cobalt phosphide multiple heterojunctions for efficient and robust photocatalyst hydrogen evolution under visible light irradiation, Renew. Energy 131 (2019) 180-186.
37. S. S. Yi, J. M. Yan, B. Wulan, S. J. Li, K. H. Liu, Q. Jiang, Noble-metal-free cobalt phosphide modified carbon nitride: an efficient photocatalyst for hydrogen generation, Appl. Catal. B 200 (2017) 477-483.
38. D. S. Dai, H. Xu, L. Ge, C. C. Han, Y. Q. Gao, S. S. Li, Y. Lu, In-situ synthesis of CoP co-catalyst decorated $Zn_{0.5}Cd_{0.5}S$ photocatalysts with enhanced photocatalytic hydrogen production activity under visible light irradiation, Appl. Catal. B 217 (2017) 429-436.
39. L. L. Wang, G. G. Tang, S. Liu, H. L. Dong, Q. Q. Liu, J. F. Sun, H. Tang, Interfacial active-site-rich

0D Co_3O_4/1D TiO_2 p-n heterojunction for enhanced photocatalytic hydrogen evolution, Chem. Eng. J. 428 (2022) 131338.
40. S. Cao, Y. Chen, H. Wang, J. Chen, X. H. Shi, H. M. Li, P. Cheng, X. F. Liu, M. Liu, L. Y. Piao, Ultrasmall CoP nanoparticles as efficient cocatalysts for photocatalytic formic acid dehydrogenation, Joule 2 (2018) 549-557.
41. X. C. Wang, K. Maeda, X. F. Chen, K. Takanabe, K. Domen, Y. D. Hou, X. Z. Fu, M. Antonietti, Polymer semiconductors for artificial photosynthesis: Hydrogen evolution by mesoporous graphitic carbon nitride with visible light, J. Am. Chem. Soc. 131 (2009) 1680-1681.
42. L. Tian, S. X. Min, F. Wang, Integrating noble-metal-free metallic vanadium carbide cocatalyst with CdS for efficient visible-light-driven photocatalytic H_2 evolution, Appl. Catal. B 259 (2019) 118029.
43. J. M. Yu, X. P. Gao, G. Z. Chen, X. X. Yuan, Electrocatalytic performance of commercial vanadium carbide for oxygen reduction reaction, Int. J. Hydrogen Energy 41 (2016) 4150-4158.

Posted on 31 Jan 2024 — The copyright holder is the author/funder. All rights reserved. No reuse without permission. — https://doi.org/10.22541/au.170669107.72727336/v1 — This is a preprint and has not been peer-reviewed. Data may be preliminary.